CR

IN-02

84123

p. 30

NI

DEVELOPMENT OF DIRECT-INVERSE 3-D METHODS FOR APPLIED AERODYNAMIC DESIGN AND ANALYSIS

Semiannual Progress Report

January 1, 1987 - June 30, 1987

AEROSPACE ENGINEERING DEPARTMENT

TAMRF Report No. 5373-87-02

July 1987

TEXAS A&M UNIVERSITY

NASA Grant No. NAG-1-619

Leland A. Carlson
Professor of Aerospace Engineering
Texas A&M University
College Station, Texas 77843-3141

TEXAS ENGINEERING EXPERIMENT STATION

DEVELOPMENT OF DIRECT-INVERSE 3-D METHODS FOR APPLIED AERODYNAMIC DESIGN AND ANALYSIS

Semiannual Progress Report

January 1, 1987 -- June 30, 1987

TAMRF Report No. 5373-87-02

July 1987

NASA Grant No. NAG-1-619

Leland A. Carlson
Professor of Aerospace Engineering
Texas A&M University
College Station, 77843-3141

DEVELOPMENT OF DIRECT-INVERSE 3-D METHODS

FOR APPLIED TRANSONIC AERODYNAMIC DESIGN AND ANALYSIS

I. Introduction

This report covers the period from Janaury 1, 1987 thru June 30, 1987. The primary tasks during this period were the completion of tasks associated with the first phase of the project, the initiation of work involving viscous interaction effects, and the continued development and testing of design methods.

II. Personnel

The staff associated with this project during the present reporting period were:

Leland A. Carlson, Principal Investigator

January thru May, Approximately 1/8 time

June -- Approximately 3/4 time

Thomas Gally, Graduate Research Assistant

January thru June

Robert Ratcliff, Graduate Research Assistant

June --

It should be noted that the first phase of the research work associated with this project has formed the basis for the Masters Thesis of Mr. Gally, who received his M.S. degree in Aerospace Engineering in

May. It is planned to use the research in the second phase of the project as the basis for the thesis of Mr. Ratcliff.

III. Research Progress

As indicated above, the primary task during this reporting period has been to "complete" the first phase of the project, which was to develop a versatile inviscid direct-inverse wing design method and program. The work in this area is presented in detail in Reference 1 and is summarized in Reference 2. A copy of Ref. 1 has been sent to NASA and Ref. 2 is included as an appendix to this report.

As part of this work, the methodology of handling surface relofting has been improved so that the method can now treat two difficult design tasks. The first task was to change a wing from super-critical to sub critical, which requires large changes in the leading edge region through relofting; and the second task was to make large surface changes to an orginal set of airfoil sections without generating errors due to a large number of geometry calculations. These objectives have been successfully demonstrated and are presented as "Test Case F" in the paper included in the Appendix. In this example, the wing for the Lockheed Wing-Body A planform at supercritical conditions was changed from a tapered thickness ranging from 12% to 6% to a 6% thick subcritical wing. Currently, efforts are in progress to go the other direction and design a supercritical thick wing starting from a thin subcritical set of airfoil sections.

Also, during this reporting period, work has begun on including viscous interaction effects in the design process. In the present context, it is planned to include as part of the viscous interaction effects the wing surface boundary layer, the wake thickness, and the wake curvature, either individually or together. Some preliminary viscous results are shown on Figures 1-4.

Figure 1 shows the design situation, which is very similar to Design Case C discussed in the Appendix. For this case, two discontinuous wing sections were designed using pressures obtained from a viscous analysis of a preselected wing planform. The wing sections consisted of NACA 0012 sections outside the design regions and modified NACA 0012 sections within the design regions. The pressures obtained from the analysis are shown in Figure 2 for a Reynolds number of approximately 11 million along with the inviscid analysis pressures used for Design Case C. The effect of including the viscous interaction can easily be seen in the more forward location and weaker shock strength for the viscous case, particularly at the outboard stations.

Figure 3 compares the initial, target, and final design surfaces for this case. As can be seen, the target surfaces were accurately obtained for each section in the inverse region. However, slight deviations were present near the trailing edges on the stations bordering the direct-analysis regions. While this phenomena has been observed for inviscid cases and is believed to be due to spanwise slope variations, the deviation for this case was more pronounced. In addition, detailed examination of several inviscid cases has revealed

that sometimes there appears to be an every-other spanwise point coupling in the designed airfoil sections. The origin of both of these phenomena is not definitiely known; and, consequently, both are currently being investigated.

Of course, the proof of a successful inverse design procedure rests in having an analysis of the designed wing predict the pressures originally desired. Such a comparison is shown on Figure 4; and, as can be seen, the agreement is quite good for preliminary design.

Another effort which has been initiated during this reporting period has been the development of an additional design strategy option to the program. Currently, the method inputs pressures at arbitrary stations, linearly interpolates these to the appropriate computational grid points within the inverse region, and calculates inverse boundary conditions and surface changes at each of these points. The new option will specify inverse boundary conditions and will calculate surface changes (i.e. new airfoil sections) only along grid lines for which a pressure distribution has been input. If there are grid lines inbetween these two sections, then that region will be treated using analysis type of boundary conditions. However, each time the boundary airfoil sections are updated, the sections inbetween will be updated using linear interpolation. Thus, in this option, the user will only specify pressure distributions at the inboard and outboard stations of the design region; and the new airfoil sections in the design region will vary smoothly along with, hopefully, the resultant pressure distributions.

While this effort is still in the developmental stage and no results are yet available, if it is successful it may offer several advantges. First, the new input format of inputting pressures at the computational grid lines, may ease the current sensitivity of the method to input pressure distributions, particularly when shock waves are included and when the present method linearly interpolates to obtain values at grid lines. Second, and perhaps most importantly, this option may be more applicable to many engineering situations and computationally faster.

IV. Future Efforts

During the next reporting period it is anticipated that most of the viscous interaction developmental work and new design option work will be completed. In addition, it is hoped that detailed verification studies can be started.

V. Grant Monitor

The NASA Technical Monitor for this project is Richard L. Campbell, Applied Aerodynamics Group, NTF Aerodynamics Branch, Transonic Aerodynamics Division, NASA Langley.

VI. References

1. Gally, Thomas A., "Inverse Transonic Wing Design Using Finite Volume Methods in Curvilinear Coordinates," M. Sc. Thesis, Texas A&M University, College Station, Tx., May 1987.

2. Gally, T. A. and Carlson, L. A., "Inviscid Transonic Wing Design Using Inverse Methods in Curvilinear Coordinates", AIAA Paper No. 87-2551CP, Proceedings of the AIAA Applied Aerodynamics Conference, American Institute of Aeronautics and Astronautics, New York, N.Y., August 1987.

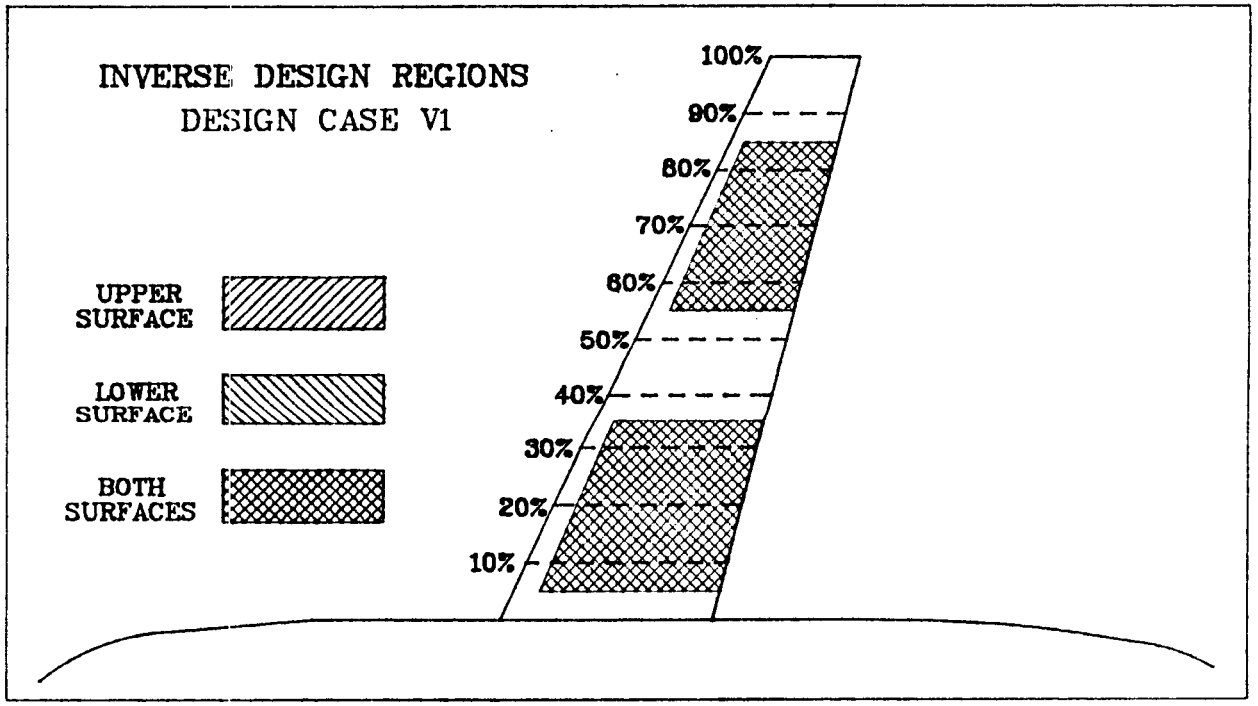

Figure 1. Design Case V1

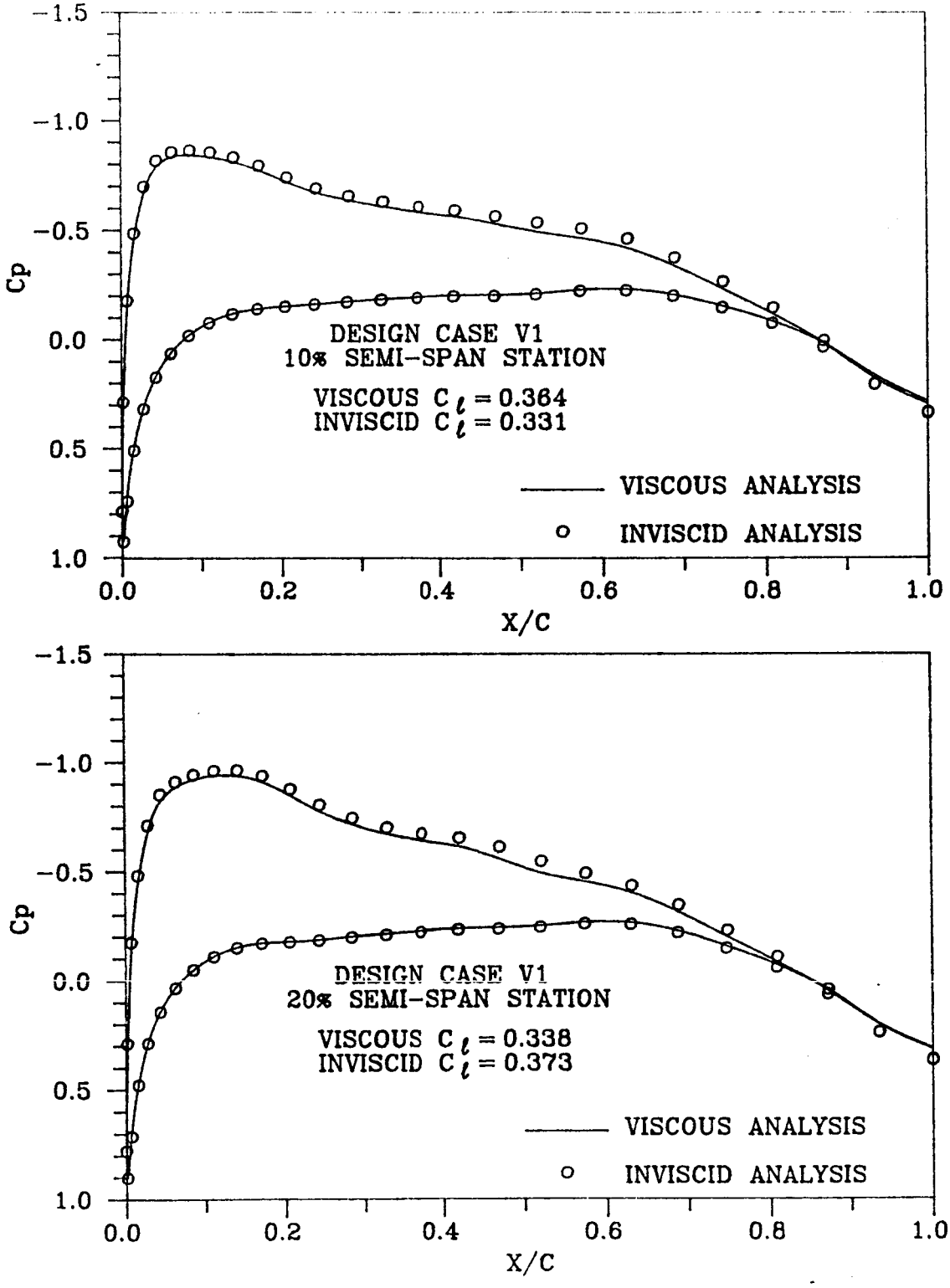

Figure 2. Comparison of Inviscid Solution and Viscous Solution (Re = 11.5 million)

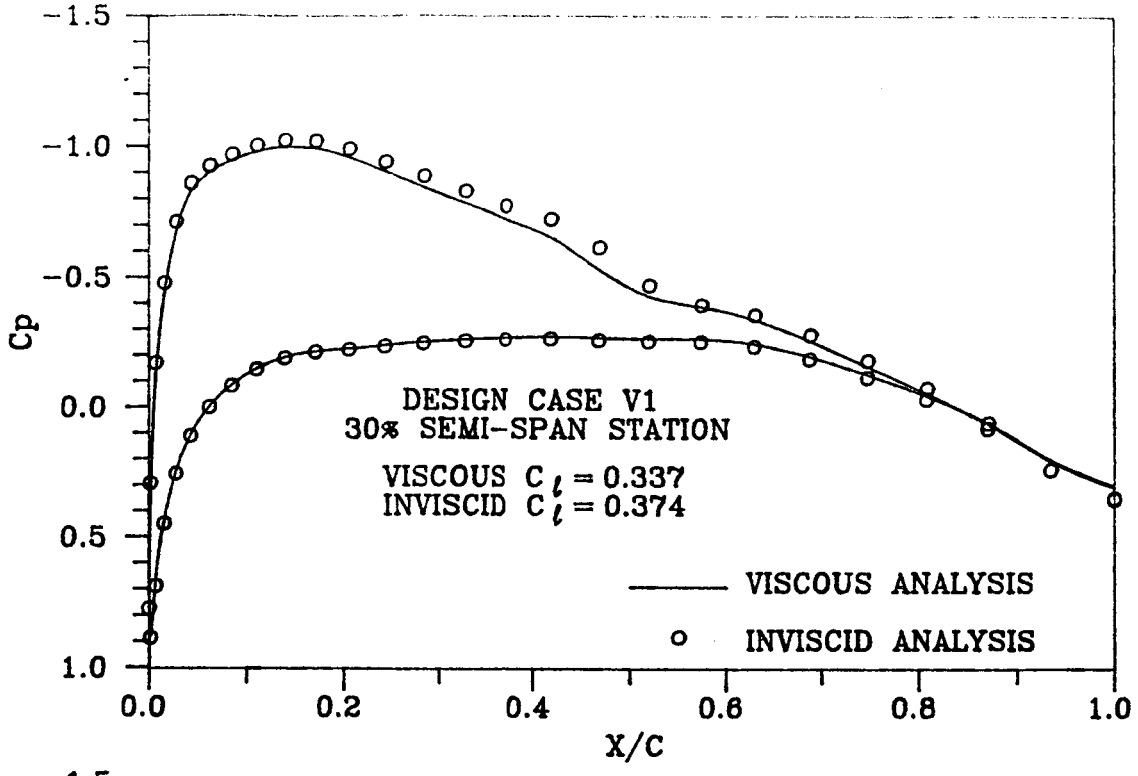

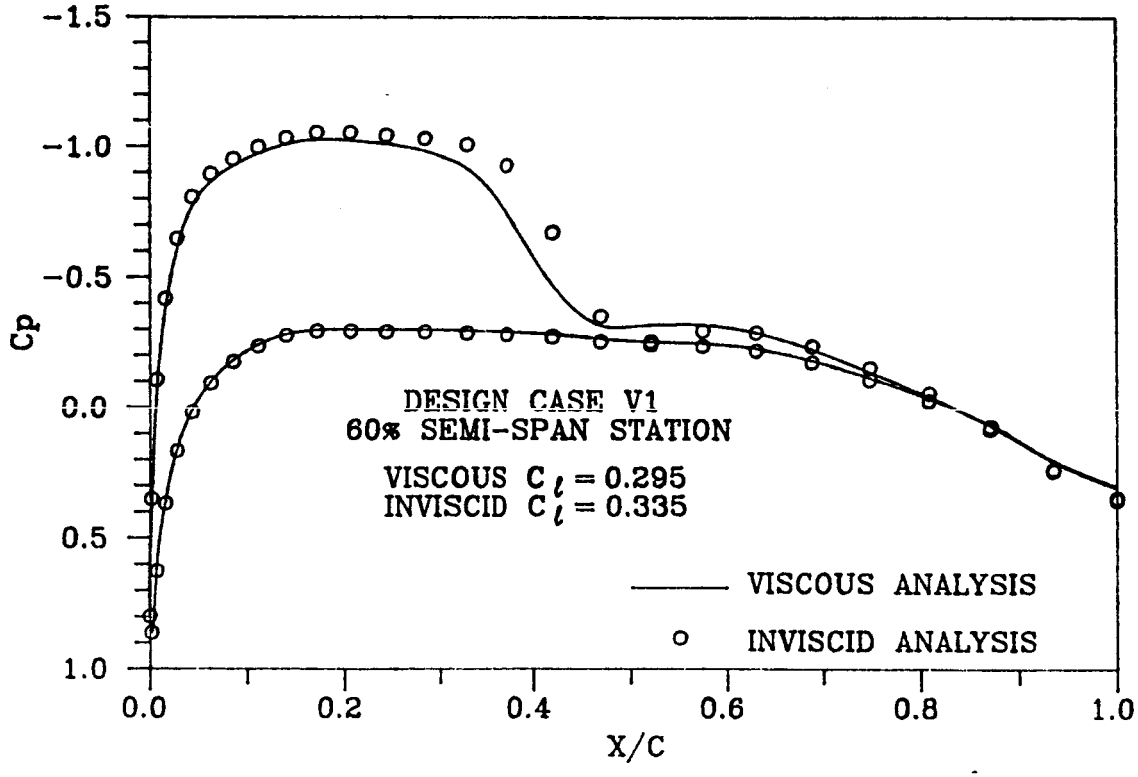

Figure 2. Continued

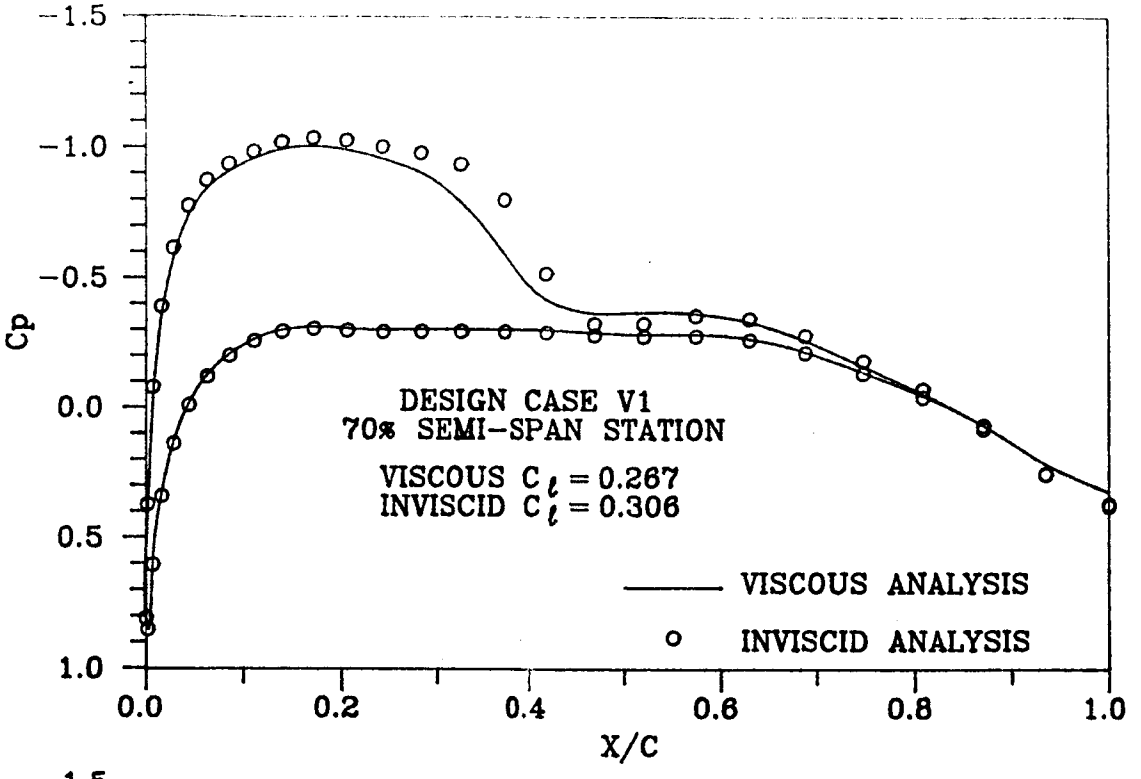

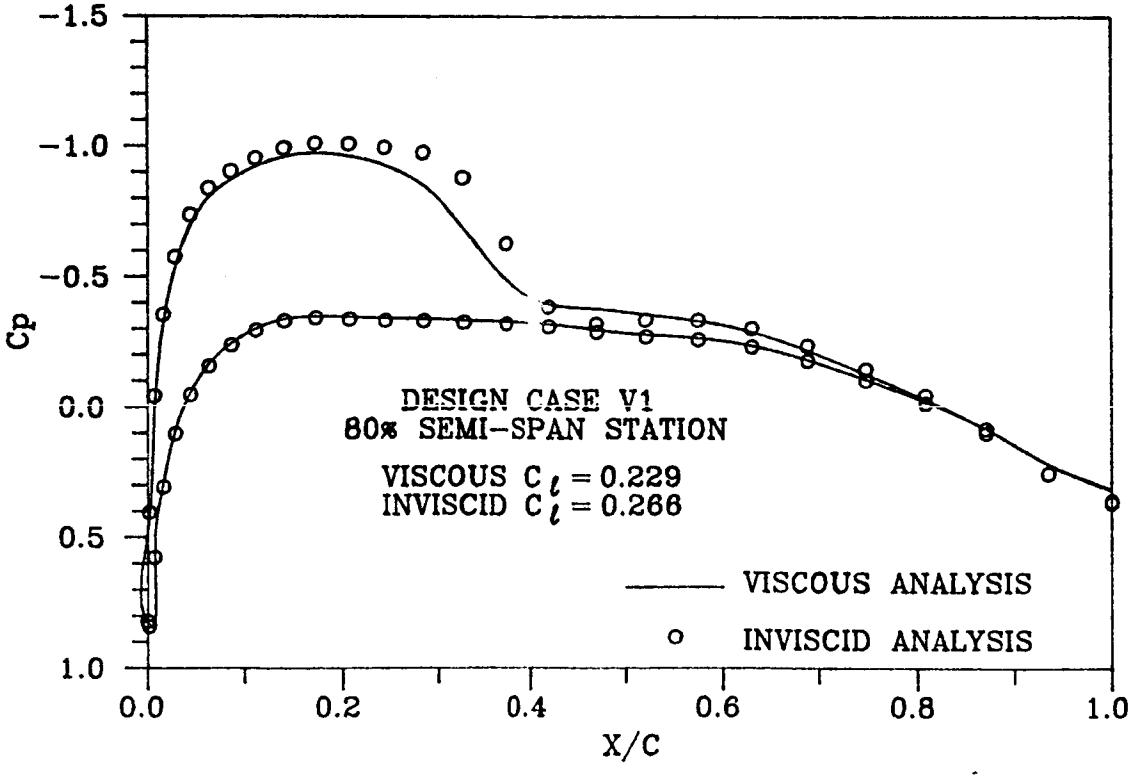

Figure 2. Continued

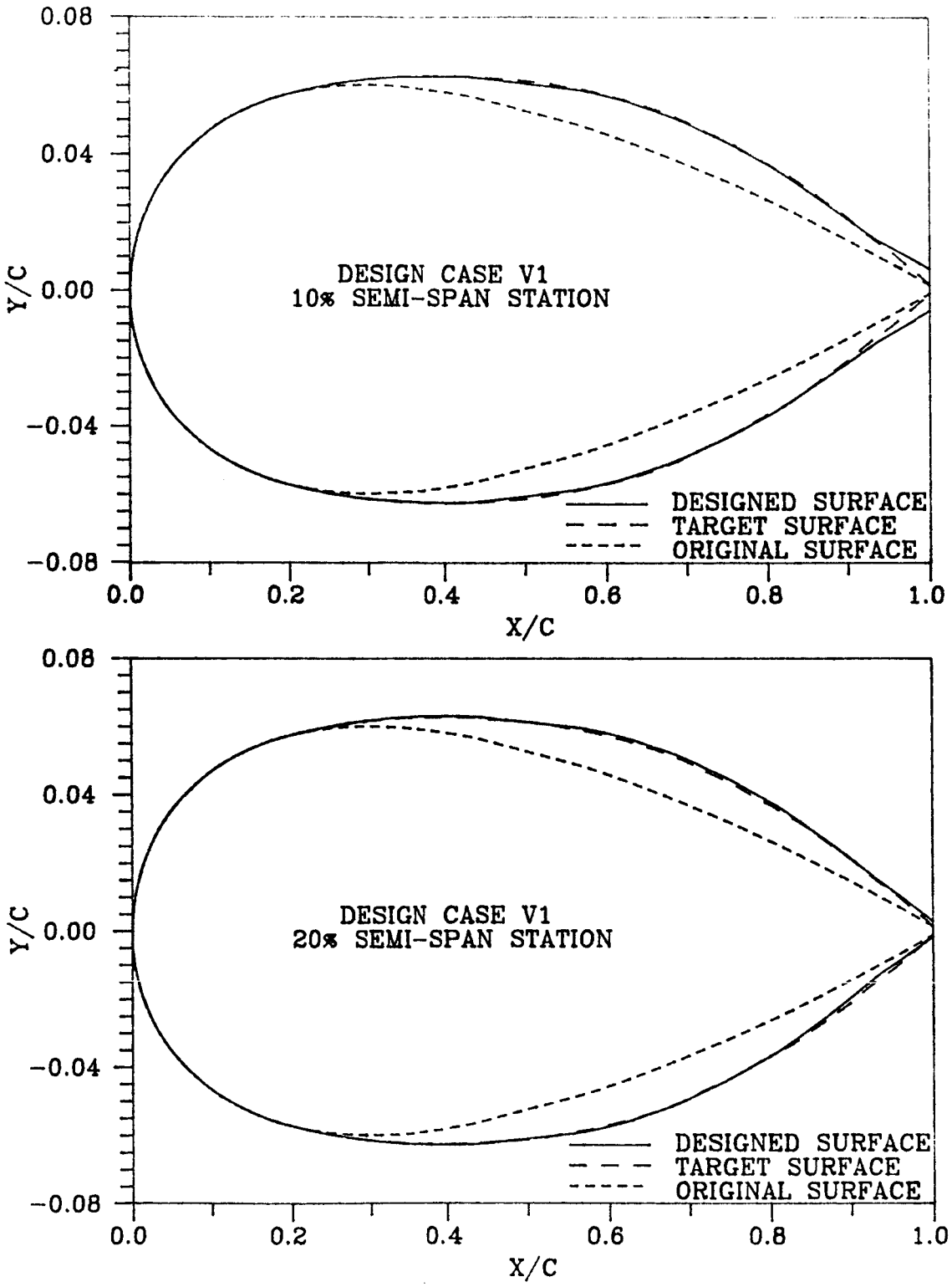

Figure 3. Comparison of Final Design Surface with Target and Initial Surfaces (Design Case V1)

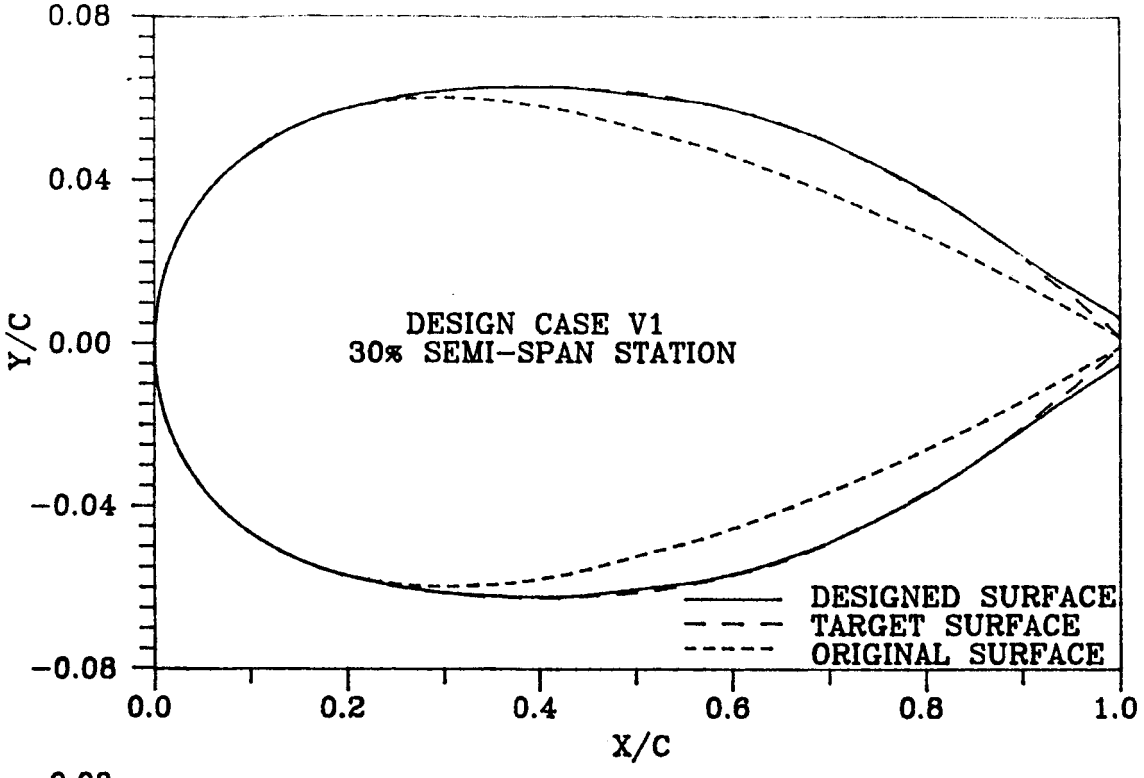

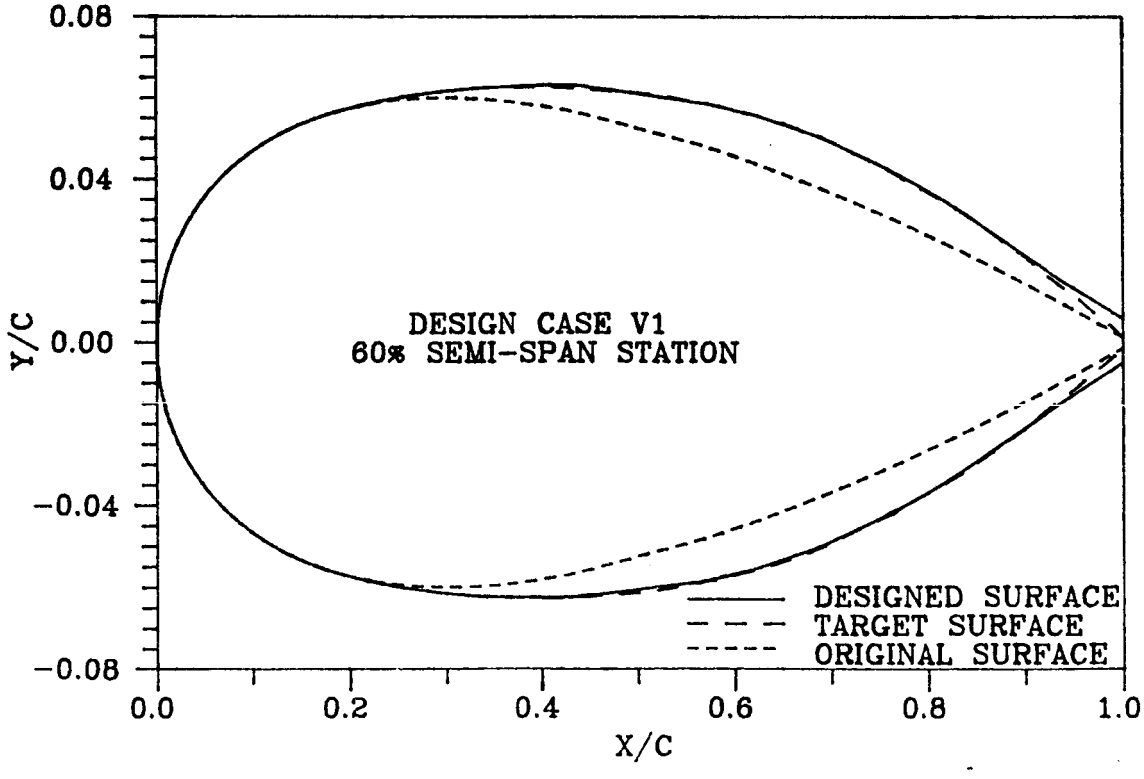

Figure 3. Continued

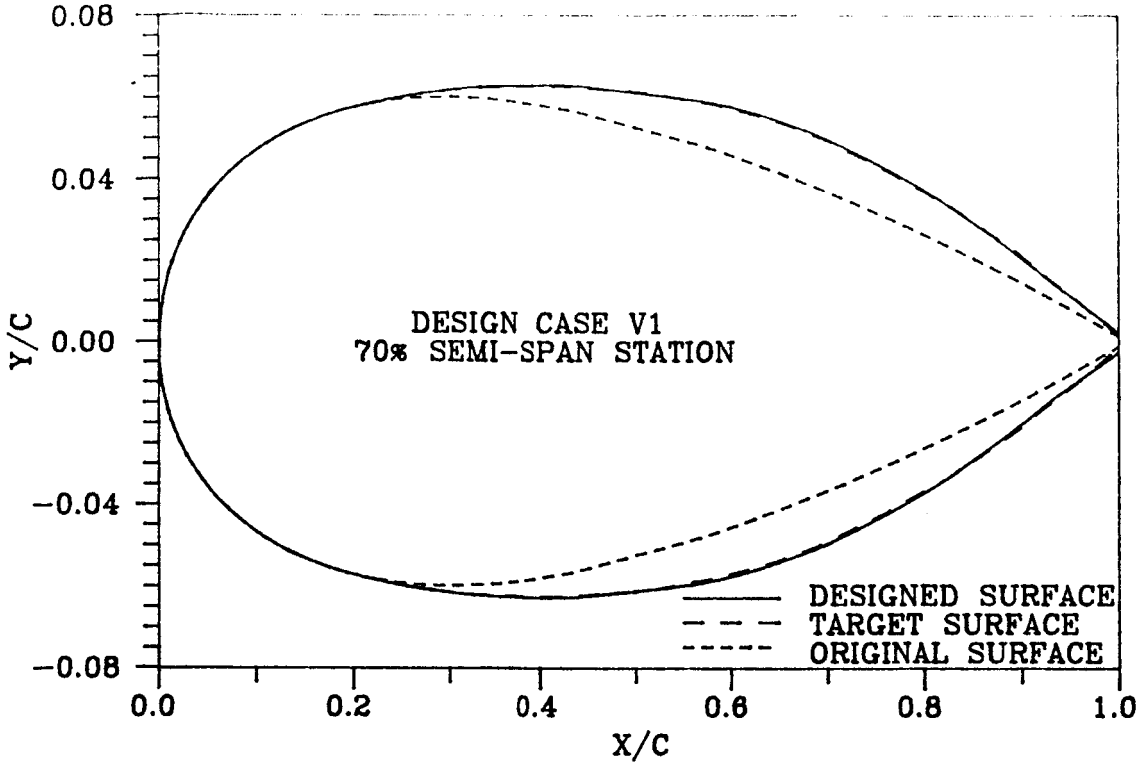

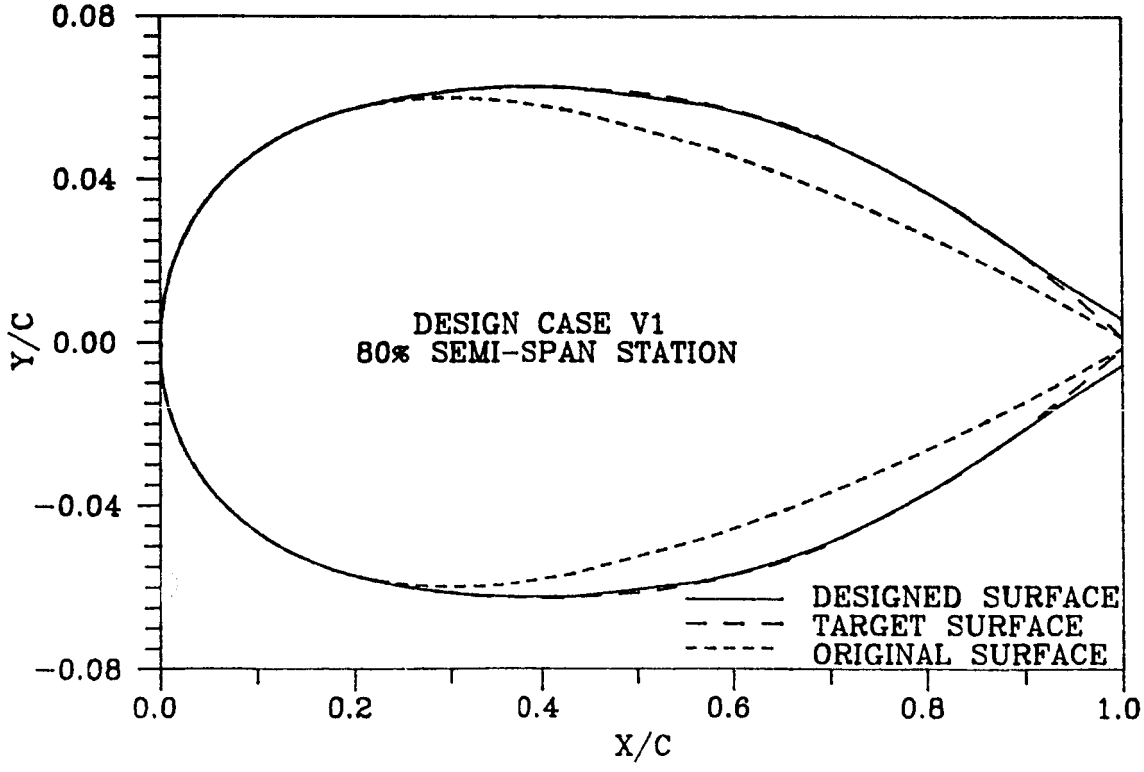

Figure 3. Continued

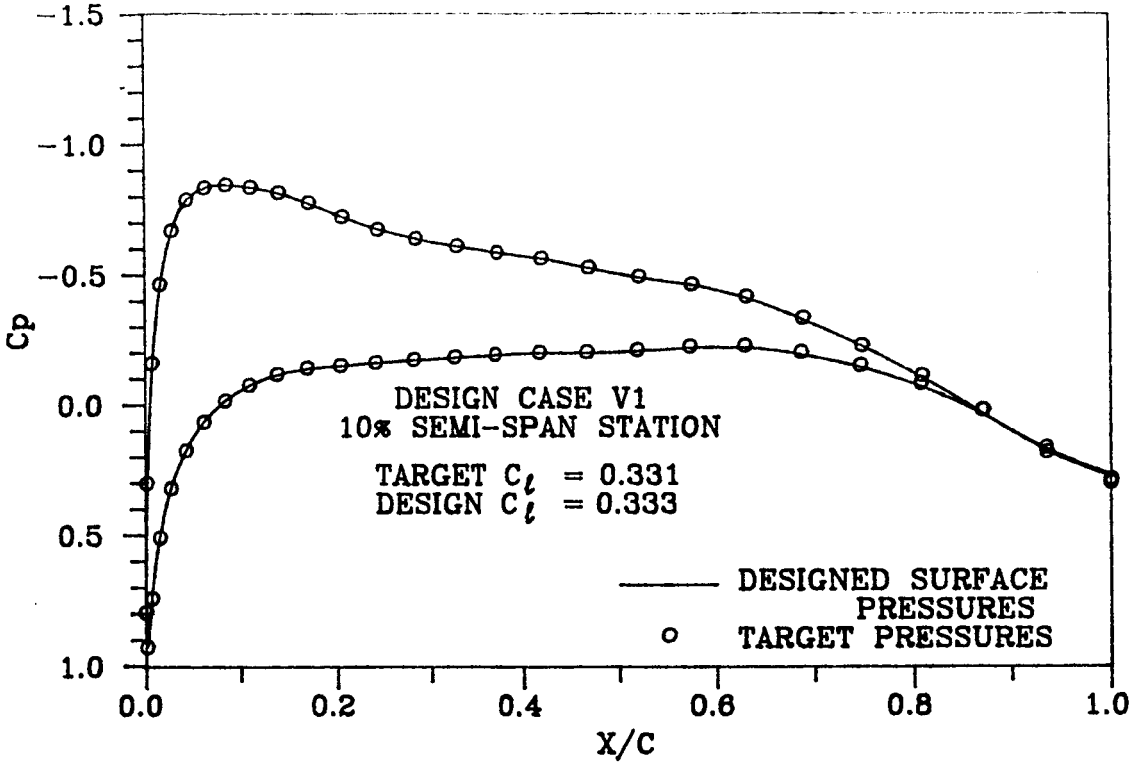

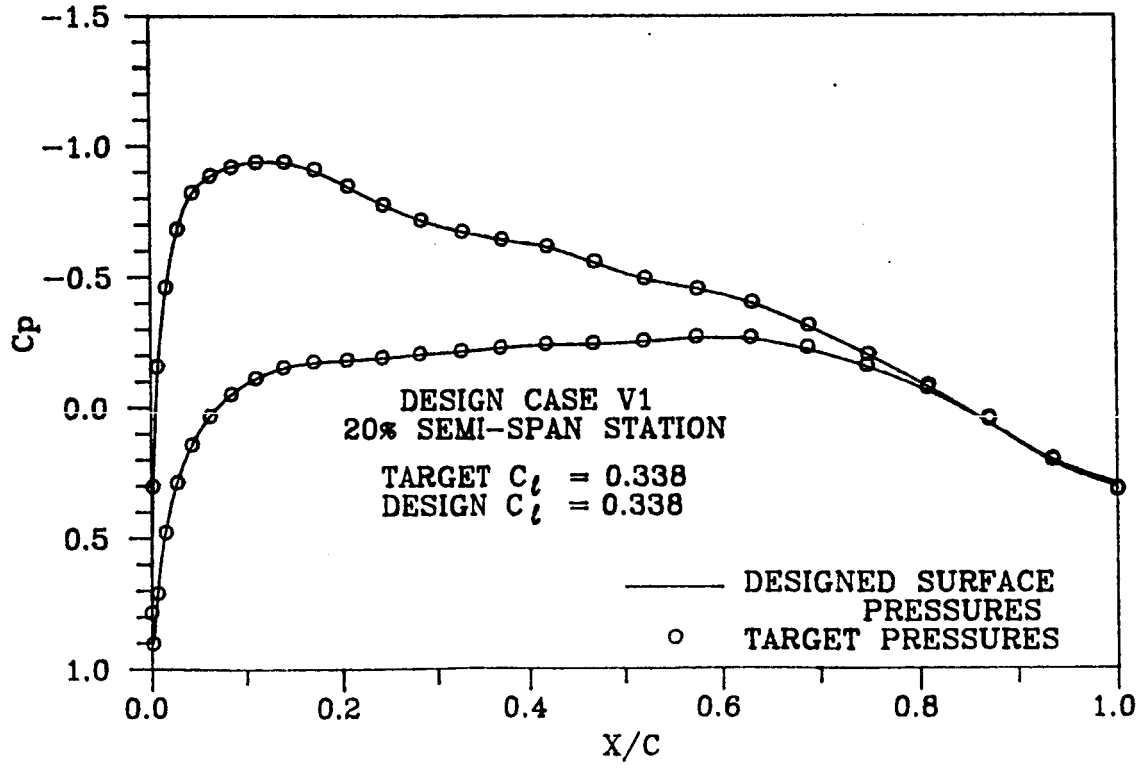

Figure 4. Comparison of Design Surface Pressures with Target Pressures (Design Case V1)

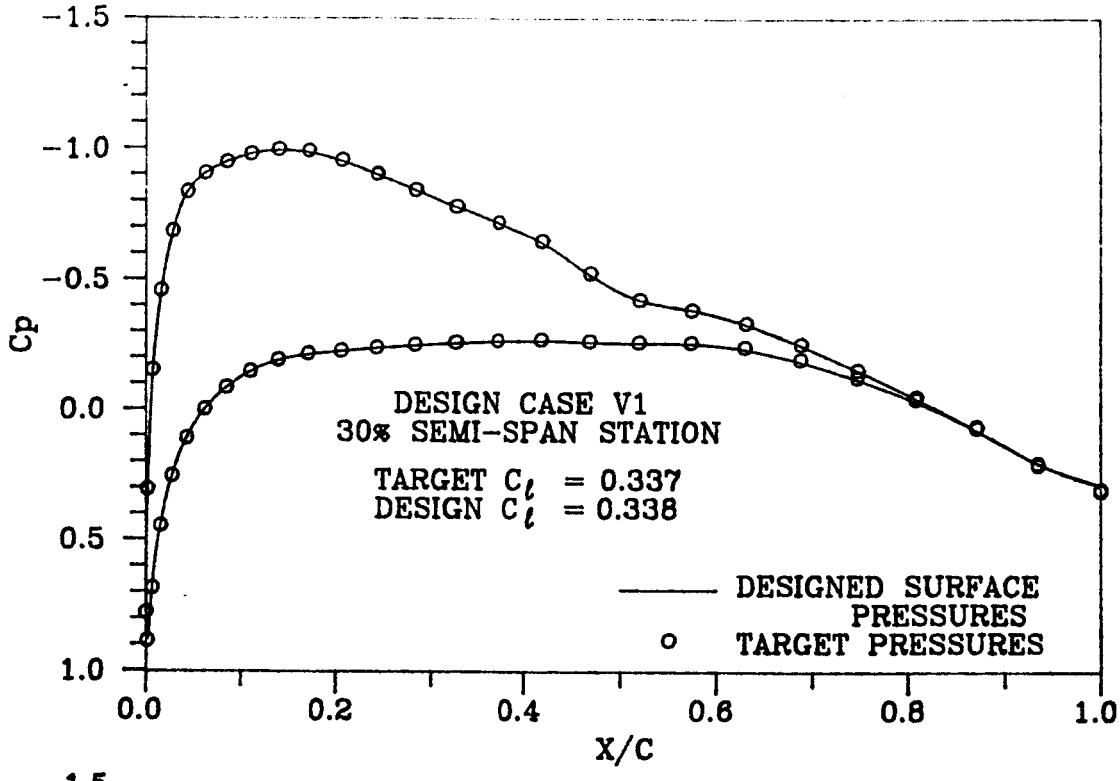

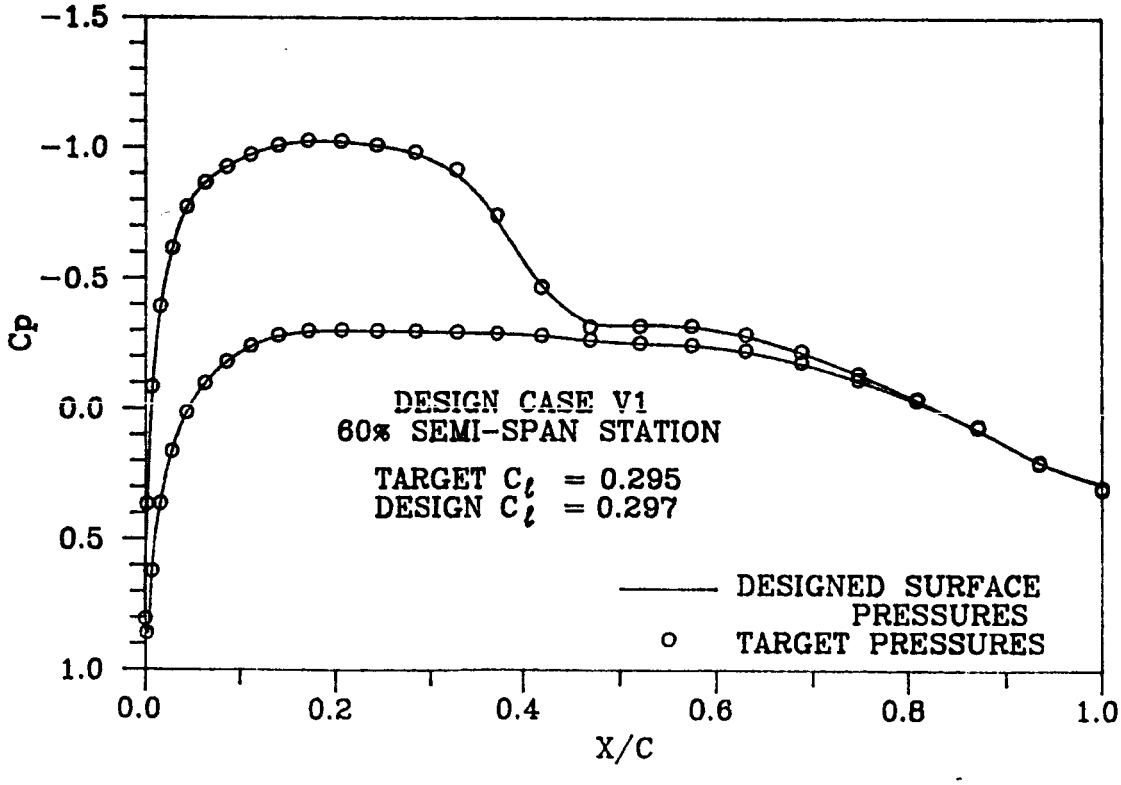

Figure 4. Continued

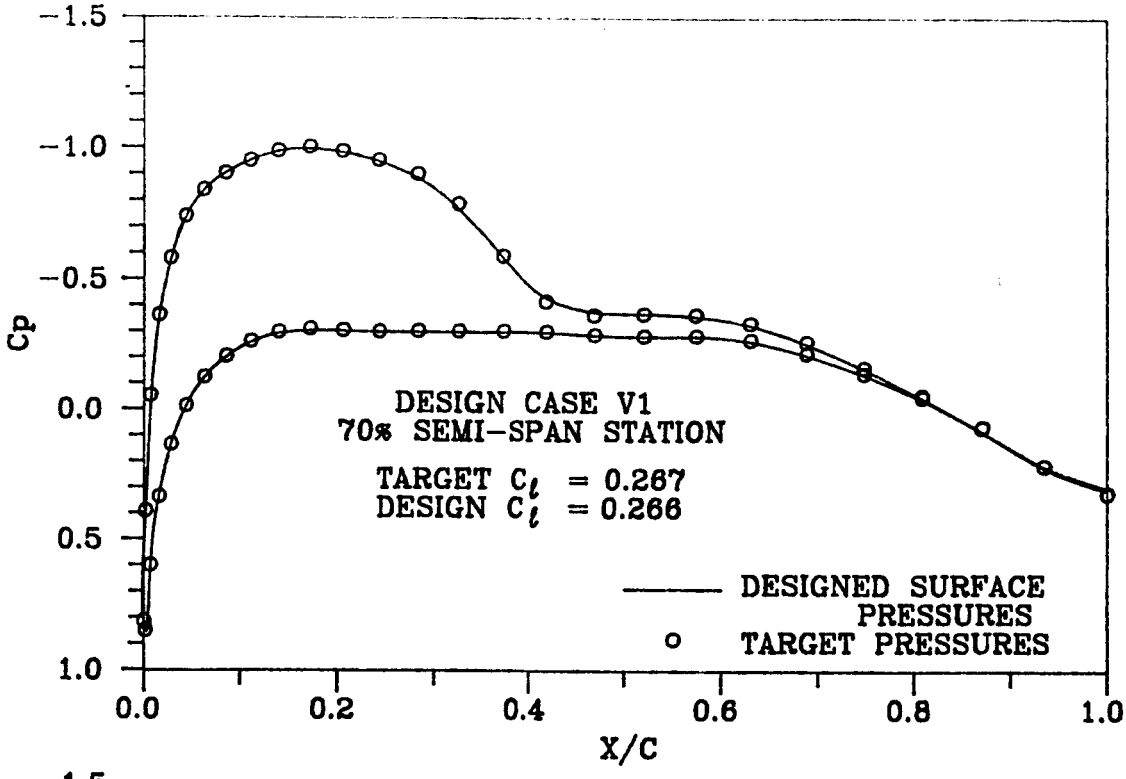

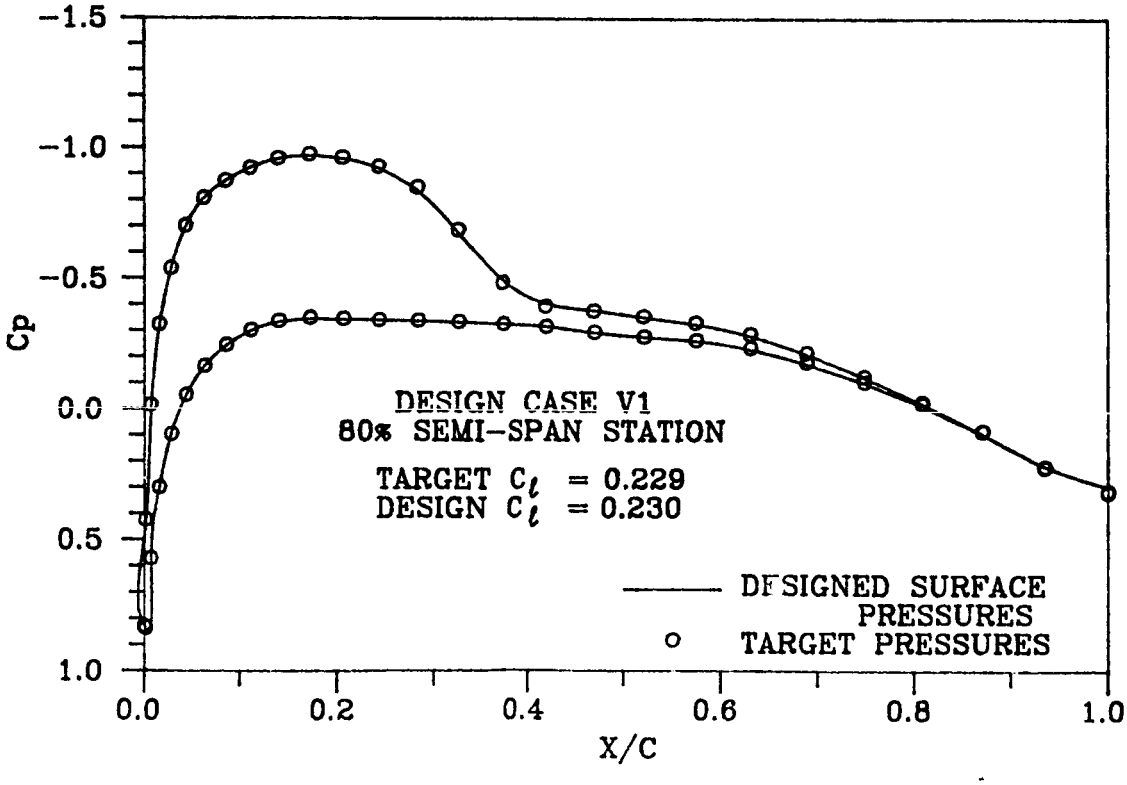

Figure 4. Continued

APPENDIX A: To be Presented as

Paper 87-2551
5th Applied Aerdynamics Conference
Monterey, California

INVISCID TRANSONIC WING DESIGN USING INVERSE METHODS IN CURVILINEAR COORDINATES

Thomas A. Gally*
Texas A&M University
College Station, Texas

Leland A. Carlson**
Texas A&M University
College Station, Texas

ABSTRACT

An inverse wing design method has been developed around an existing transonic wing analysis code. The original analysis code, TAWFIVE, has as its core the numerical potential flow solver, FLO30, developed by Jameson and Caughey. Features of the analysis code include a finite-volume formulation; wing and fuselage fitted, curvilinear grid mesh; and a viscous boundary layer correction that also accounts for viscous wake thickness and curvature. The development of the inverse methods as an extension of previous methods existing for design in Cartesian coordinates is presented. Results are shown for inviscid wing design cases in super-critical flow regimes. The test cases selected also demonstrate the versatility of the design method in designing an entire wing or discontinuous sections of a wing.

NOMENCLATURE

C_p	- Coefficient of pressure
h	- Jacobian of coordinate transformation
H	- Jacobian matrix
J	- Transpose of inverse Jacobian matrix
M_∞	- Freestream Mach number
q_∞	- Magnitude of freestream velocity
Q	- Magnitude of local velocity
u,v,w	- Components of physical velocity vector
U,V,W	- Components of contravariant velocity vector
α	- Angle of attack
γ	- Ratio of specific heats
δ	- Differential operator
$\delta(x)$	- Displacement thickness
$\delta_r(x)$	- Displacement thickness due to relofting
Δ	- Trailing edge thickness
Δ_t	- User specified trailing edge thickness
μ	- Averaging operator
ρ	- Density
ϕ	- Reduced/perturbation potential function ($\Phi = \phi + x\cos(\alpha) + y\sin(\alpha)$)
Φ	- Potential function

INTRODUCTION

In recent years the importance of transonic flight to both military and commercial aircraft and the development of specialized transonic wings for several flight research experiments have prompted significant efforts to develop accurate and reliable computational methods for the analysis and design of transonic wings. Many methods of solution have been developed, but among those which have shown promise due to their computational efficiency and engineering accuracy have been those based upon the full potential flow equations in either their conservative or non-conservative form[1-3]. The TAWFIVE[4] FORTRAN code in particular has proven to be an excellent and reliable analysis tool. This analysis code is based upon the FLO30 finite volume potential flow method that was developed by Jameson and Caughey[3]. Among the features of FLO30 are its fully conservative formulation and its three-dimensional curvilinear grid. The latter can be fit around any general combination of fuselage shape and wing planform.

The purpose of the research described in this paper has been to develop a wing design method that is based on the existing TAWFIVE analysis code and is compatible with the existing computational methods and program structure of that code. Of the many wing and airfoil design methods available[5-8], the inverse method as developed by Carlson[9-12] was selected for use. The current work extends the previously developed design methods developed for orthogonal grids to the more generalized curvilinear grid system of TAWFIVE, while also providing greater design flexibility and versatility for engineering applications. These last goals were achieved by the inclusion of user options for designing either the entire wing or only discontinuous wing segments as shown in Figure 1. The availability of this option is useful to engineers who are typically faced with designing around regions where the wing geometry may be fixed by constraints other than aerodynamic considerations.

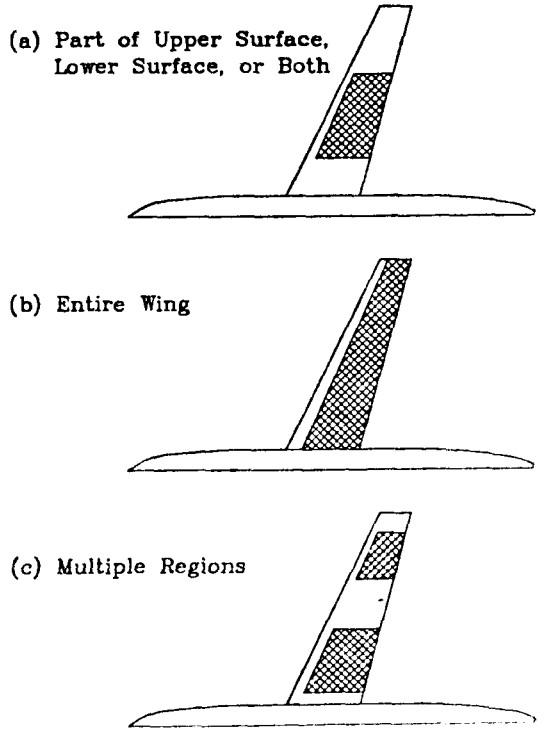

Figure 1. Possible Wing Design Situations

* Graduate research assistant.
** Professor of Aerospace Engineering, Associate Fellow of AIAA

WING ANALYSIS METHODS

Potential Flow Solver

The inviscid potential analysis of TAWFIVE is performed by the program FLO30 developed by Caughey and Jameson[3,13]. For a complete description of the FLO30 code and its theoretical basis the reader is referred to Caughey and Jameson's papers and some earlier developmental work by Jameson[14-15]. A brief description is presented here to provide for completeness and to provide a background for the inverse design developments which will be discussed in detail.

FLO30 solves the full potential equation in conservative form which when transformed from Cartesian coordinates to generalized curvilinear coordinates is:

$$(\rho hU)_\xi + (\rho hV)_\eta + (\rho hW)_\zeta = 0 \qquad (1)$$

where the subscripts denote differentiation with respect to the curvilinear coordinates ξ, η, and ζ. The contravariant velocities are related to the physical velocities and the derivatives of the potential function by:

$$\begin{Bmatrix} U \\ V \\ W \end{Bmatrix} = H^{-1} \begin{Bmatrix} u \\ v \\ w \end{Bmatrix} = (H^T H)^{-1} \begin{Bmatrix} \Phi_\xi \\ \Phi_\eta \\ \Phi_\zeta \end{Bmatrix} \qquad (2)$$

and H is the transformation matrix defined by:

$$H = \begin{bmatrix} x_\xi & x_\eta & x_\zeta \\ y_\xi & y_\eta & y_\zeta \\ z_\xi & z_\eta & z_\zeta \end{bmatrix} \quad \text{with} \quad h = |H| \qquad (3)$$

The local density can be obtained from isentropic relations as:

$$\rho = [1 + \tfrac{\gamma-1}{2} M_\infty^2 (1 - u^2 - v^2 - w^2)]^{\frac{1}{\gamma-1}} \qquad (4)$$

The numerical approach used in FLO30 is a finite volume technique. To understand this approach, consider the simple two dimensional case represented by the grid system shown in Figure 2.

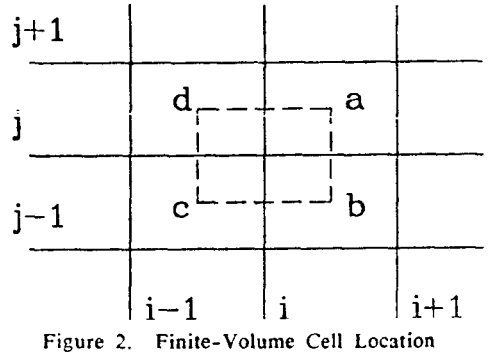

Figure 2. Finite-Volume Cell Location

The dashed cube shown in the figure indicates the area element under consideration. The flux of fluid through side a-b can be approximated by the average of the fluxes at point a and b with similar results for the side c-d. The net flux in the x direction for the elemental area centered at grid point i,j is then:

$$(\rho hU)_\xi = [(\rho hU_a + \rho hU_b) - (\rho hU_c + \rho hU_d)] \,/\, 2\Delta\xi$$

or in the notation of Caughey and Jameson,

$$(\rho hU)_\xi = \mu_\eta \delta_\xi (\rho U)$$

where μ indicates averaging and δ indicates differentiation in the indicated directions which are defined as follows (allowing $\Delta\xi=\Delta\eta=\Delta\zeta=1$):

$$(\delta_\xi U)_{i,j,k} = (U_{i+\frac{1}{2},j,k} - U_{i-\frac{1}{2},j,k})$$
$$(\mu_\xi U)_{i,j,k} = (U_{i+\frac{1}{2},j,k} + U_{i-\frac{1}{2},j,k})/2$$
$$(\mu_{\xi\eta} U)_{i,j,k} = (U_{i+\frac{1}{2},j+\frac{1}{2},k} + U_{i+\frac{1}{2},j-\frac{1}{2},k} + U_{i-\frac{1}{2},j+\frac{1}{2},k} + U_{i-\frac{1}{2},j-\frac{1}{2},k})/4$$
$$\ldots \text{ etc.}$$

When extended to the other flux components and to averaging over cube surfaces in three dimensions, the numerical potential equation is of the form:

$$\mu_{\eta\zeta}\delta_\xi(\rho hU) + \mu_{\zeta\xi}\delta_\eta(\rho hV) + \mu_{\xi\eta}\delta_\zeta(\rho hW) = 0$$

To find the flux quantities ρhU, ρhV, and ρhW at the finite volume cell vertices (i.e. points a, b, c, and d for the two dimensional case), it is necessary to evaluate Equations (2) through (4). The derivatives in these expressions can be expanded by the same volume averaging approach used above, thus:

$$\Phi_\xi = \mu_{\eta\zeta}\delta_\xi(\Phi) \qquad x_\xi = \mu_{\eta\zeta}\delta_\xi(x)$$
$$\Phi_\eta = \mu_{\zeta\xi}\delta_\eta(\Phi) \qquad y_\xi = \mu_{\eta\zeta}\delta_\xi(y)$$
$$\Phi_\zeta = \mu_{\xi\eta}\delta_\zeta(\Phi) \qquad z_\xi = \mu_{\eta\zeta}\delta_\xi(z)$$

with similar terms for the other transformation metrics. The above expressions, being centered at grid midpoints, will involve the values of the potential and grid position at grid points which are known from the previous potential solution and the grid geometry, respectively.

When solving transonic flows it is necessary to include in the solution algorithm some form of supersonic upstream dependence in order to account for both the physical nature of the flow and the viscous nature of shock waves, respectively. Caughey and Jameson introduced upwinding by the addition of terms into their potential numerical equation which are only non-zero when the flow is supersonic. Also, the finite volume technique exhibits a tendency for uncoupling of the flow field solution between alternating grid points. As a result, additional terms are included in the numerical potential equation. The final numerical equation which is solved by FLO30 when these terms have been included has the form:

$$\mu_{\eta\zeta}\delta_\xi(\rho hU+P) + \mu_{\zeta\xi}\delta_\eta(\rho hV+Q) + \mu_{\xi\eta}\delta_\zeta(\rho hW+R) - \epsilon(\mu_{\zeta}\delta_{\xi\eta}Q_{\xi\eta} + \mu_{\xi}\delta_{\eta\zeta}Q_{\eta\zeta} + \mu_{\eta}\delta_{\zeta\xi}Q_{\zeta\xi} - \delta_{\xi\eta\zeta}Q_{\xi\eta\zeta}/2) = 0$$

where P, Q, and R are the upwinding terms and $Q_{\xi\eta}$, $Q_{\eta\zeta}$, $Q_{\zeta\xi}$, and $Q_{\xi\eta\zeta}$ are the decoupling terms.

Computational Grid Geometry

The computational grid used by FLO30 is a body fitted, non-orthogonal curvilinear mesh constructed about a wing fuselage combination. The number of grid points composing the computational domain is typically 40 x 6 x 8, 80 x 12 x 16, or 160 x 24 x 32 for the number of ξ, η, and ζ points in the coarse, medium, and fine grids, respectively. The grid is conformally mapped to the wing and fuselage surfaces as can be seen from the plot of surface grid lines shown in Figure 3.

The grid is formed around spanwise airfoil sections in a similar manner in which "C" grids are mapped to airfoils in two-dimensional analysis. In addition, each spanwise computational plane is also conformally wrapped about the fuselage surface and a line extending forward from the fuselage nose.

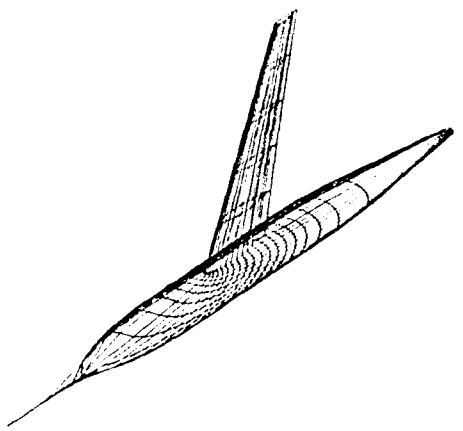

Figure 3. Surface Grid Point Geometry

A final set of grid surfaces are generated beneath the wing and fuselage surfaces and beyond the symmetric plane in order to aid in the formulation of both the finite-volume numerical flow equations and the flow tangency boundary conditions upon these boundaries. The grid points composing the "ghost" surfaces are calculated from linear extrapolations of the computation grid lines from inside the physical domain.

Boundary Conditions

Since the governing potential equations are written in terms of perturbations from free-stream conditions, the subsonic, far-field requirement that the flow return to the free-stream velocity and direction is satisfied by setting the perturbation potential equal to zero on the side and upstream boundaries. The downstream boundary condition is a "zero" order extrapolation of the potential (constant potential assumption) to the outflow boundaries.

A flow tangency condition is applied along both the wing and fuselage solid surfaces by setting the normal contravariant component of the velocity vector to zero on the surfaces. This condition provides an equation which when approximated by a finite-difference expansion about the surface grid points can be used to set a value for the perturbation potential on the "ghost" grid points below each surface. Note that this *finite-difference* boundary condition differs in formulation from the *finite-volume* solution algorithm of the governing equations. As a result, it is possible to impose flow tangency using the finite-difference technique yet still have a slight normal surface velocity when performing the finite-volume calculations. Since it is essential to have accurate boundary conditions at the wing surface in order to generate accurate solutions, a second condition is imposed upon the wing surface. This additional condition involves reflecting the flux quantities calculated by the flow solver for the cell centers directly above the wing surface to the "ghost" cell centers beneath. The reflected normal fluxes then cancel each other out in the residual expression and a net zero flow is obtained through the surface. Similarly, a zero flux condition is applied at the half body symmetric plane, limiting solutions to symmetric, non-sideslip cases.

The trailing edge slit boundary is not an actual limit to the physical domain as the other boundaries are, but is simply an artificial boundary created by unwrapping the physical plane into the computational domain. The only conditions which need to be imposed at the slit is that the flow velocities, and thus pressure, be continuous across the cut. The flow potential, however, will have a discontinuous jump across the wake which is proportional to the sectional wing lift coefficient.

INVERSE WING DESIGN METHODS

As stated previously, a direct-inverse approach to wing design was selected for incorporation into the TAWFIVE code. The direct-inverse method derives its name from the division of the design wing surface into a fixed geometry leading edge region, where flow tangency boundary conditions are imposed, and an aft, variable geometry section where pressure boundary conditions are enforced. The pressure boundary where the user specified pressure distributions are imposed does not extend forward to the leading edge due to difficulties of enforcing this type boundary condition near the beginning of an airfoil section. This restriction on the size of the pressure specification region does not seriously reduce the versatility of the design method since the leading edge regions for most airfoils are similar, and it is relatively easy to select a leading edge geometry which will produce the desired Mach number or pressure values at the beginning of the inverse region. In addition, specific leading edge shapes may be required due to other design constraints such as the necessity to house a leading edge flap or slot system.

Pressure Boundary Condition

In the inverse design regions on the wing, a pressure boundary condition will be specified rather than the flow tangency condition used in analysis zones. In formulating this boundary condition it is necessary to relate the user specified pressure coefficient, C_p, to the current perturbation potentials at inverse design grid points. Consider the full potential equation for the pressure coefficient:

$$C_p = \frac{2}{\gamma M_\infty^2}\left\{\left[1 + \frac{\gamma-1}{2} M_\infty^2\left(1 - \frac{Q^2}{q_\infty^2}\right)\right]^{\frac{\gamma}{\gamma-1}} - 1\right\}$$

where: $Q^2 = u^2 + v^2 + w^2$.

If it is assumed that the pressure coefficient is primarily a function of the chordwise component of the velocity, u, and only slightly affected by the vertical and spanwise components of velocity, v and w, then a stable approximation is made by time lagging the latter two velocities in the boundary condition expression. This assumption is true everywhere except near the leading edge; but since the inverse design boundaries have already been restricted to regions well behind the leading edge, the simplification is justified. The value of the local velocity, u, can then be calculated from the above expression in terms of the desired pressure coefficient and the current values for the vertical and spanwise velocities. In addition, the velocity u can also be calculated from the perturbation potentials using the relations of Eq. (2). Defining J_{ij} to be the elements of the inverse transpose of the Jacobian matrix, H, the two equations for u yield:

$$J_{11}\phi_\xi + J_{12}\phi_\eta + J_{13}\phi_\zeta = \frac{1 - \frac{2}{(\gamma-1)M_\infty^2}\left[\left(1 + \frac{\gamma M_\infty^2 C_p}{2}\right)^{\frac{\gamma-1}{\gamma}} - 1\right]}{1 + \left(\frac{v}{u}\right)^2 + \left(\frac{w}{u}\right)^2} - \cos(\alpha) \quad (5)$$

Since the spanwise and vertical flow velocities have already been assumed to be constant in the boundary condition relation, it is consistent to make the same approximation in the above expression with respect to the spanwise and vertical derivative terms, ϕ_η and ϕ_ζ. This assumption is similar to the previous one, and leads to an explicit expression for the potential at one point.

The finite difference approximation used involves expanding the derivatives of the potential about the mid-point i-½,j,k. The ξ derivative is determined by a central difference involving the preceding and following grid point values. The η and ζ derivatives are found at the mid-point by averaging the derivatives from the preceding and following grid points found by a three point backwards and central difference approximations, respectively. Figure 4 shows the point dependence and pressure specification point for this method. The resulting numerical expression obtained with these finite approximations is:

$$J_{11}(\phi^{n+1}_{i,j,k} - \phi^{n}_{i-1,j,k}) + J_{12}\left[3(\phi^{n+1}_{i,j,k} + \phi^{n}_{i-1,j,k}) - 4(\phi^{n}_{i,j-1,k} + \phi^{n}_{i-1,j-1,k}) + \phi^{n}_{i,j-2,k} + \phi^{n}_{i-1,j-2,k}\right]/4 + J_{13}(\phi^{n}_{i,j,k+1} + \phi^{n}_{i-1,j,k+1} - \phi^{n}_{i,j,k-1} - \phi^{n}_{i-1,j,k-1})/4 = F(Cp_{i-\frac{1}{2},k})$$

Here, the superscripts n and n+1 refer to current values of the potential and the new values of the potential being imposed by the boundary condition, respectively. Also, the term $F(Cp_{i-\frac{1}{2},k})$ is the right hand side of Eq. (5) evaluated using the pressure coefficient specified at point i-½,k. Solving the above expression for the potential at point i,j,k yields:

$$\phi^{n+1}_{i,j,k} = \frac{1}{J_{11} + 3J_{12}/4}\left\{ J_{11}\phi^{n}_{i-1,j,k} - J_{12}\left[3\phi^{n}_{i-1,j,k} - 4(\phi^{n}_{i,j-1,k} + \phi^{n}_{i-1,j-1,k}) + \phi^{n}_{i,j-2,k} + \phi^{n}_{i-1,j-2,k}\right]/4 - J_{13}(\phi^{n}_{i,j,k+1} + \phi^{n}_{i-1,j,k+1} - \phi^{n}_{i,j,k-1} - \phi^{n}_{i-1,j,k-1})/4 + F(Cp_{i-\frac{1}{2},k})\right\}$$

The potential values at n+1 in the direct region are known initially since they do not change when the inverse boundary condition is applied; *i.e.* $\phi^{n+1} = \phi^{n}$. All the potentials on the inverse boundary can then be calculat d and, since the spanwise and vertical derivatives are small, will primarily be functions of the pressure coefficient at grid point i-½ and the value of the potential at grid point i-1.

The only concern with using this mid-point specification scheme is that the current method of calculating the pressure data output from FLO30 uses a grid point centered difference scheme for the streamwise derivative. This difference could potentially allow a pressure to be specified correctly but still have a significantly different value output from FLO30 due to the inconsistent calculation methods. However, as shown on Figure 5, where the pressures calculated for a typical flow solution are compared for the two different calculation techniques, this possible error has not been significant in practice.

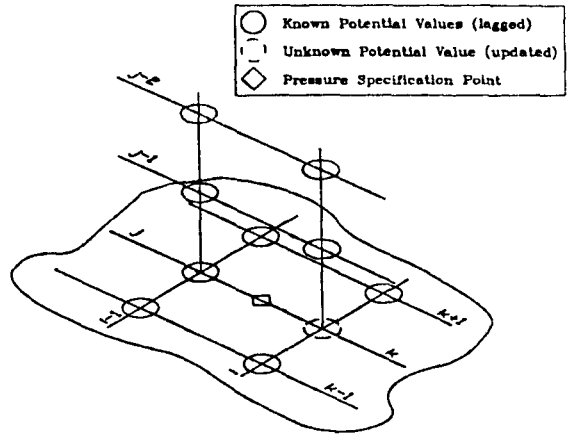

Figure 4. Point Dependance and Location

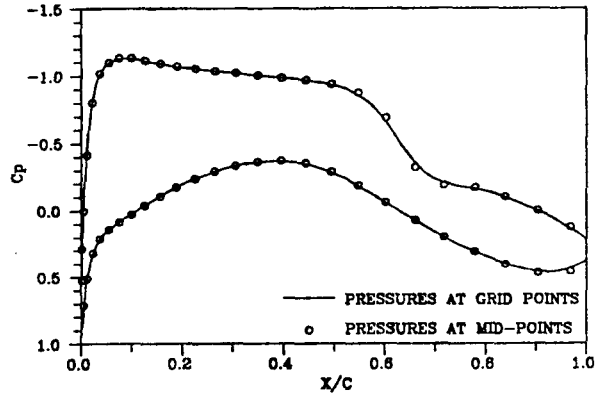

Figure 5. Comparison of Pressure Calculation Methods

Surface Calculations

As the inverse boundary conditions drive the flow field to a converged solution, it is necessary to periodically calculate the location of the new displacement surface and to regenerate the computational grid about this new geometry so that the pressure boundary surface will correspond to the physical boundary surface. Each new surface can be found relative to the previous surface from an integration of the wing surface slopes. However, the surface slopes must first be calculated from the current flow field solution using the flow tangency boundary condition which in curvilinear coordinates is:

$$V^T \times \nabla F = 0$$

where V is the contravariant velocity vector and ∇F is the gradient of the surface function with respect to the curvilinear coordinates. Note this condition is a direct analog to the same condition expressed in physical space.

A more useful expression can be obtained by expanding the above equation to:

$$\left(\frac{\partial \eta}{\partial \xi}\right)_{wing} = \frac{V}{U} - \frac{W}{U}\left(\frac{\partial \eta}{\partial \zeta}\right)_{wing}$$

This expression can be solved for the new chordwise

airfoil slopes, $\partial\eta/\partial\xi$, if the current values of the spanwise slope, $\partial\eta/\partial\zeta$, are used. Since the wing surface is represented in the computational grid as a plane of constant η, the current slopes on the wing surface equal zero and a simplified flow tangency condition results:

$$\left(\frac{\partial\eta}{\partial\xi}\right)_{\text{wing}} = \frac{V}{U}$$

The above expression has been applied to the computational surface plane in order to find the relative location of the new physical surface. This approach is an approximation since the above equation is only exactly true when applied to the new surface itself. Using this method, however, provides for a stable iterative surface updating procedure which quickly converge to the target surface.

To calculate the relative surface slopes, it is first necessary to accurately determine the values of the contravariant velocities, U and V. As was also determined by the work of Weed, et al.[12], a simple finite difference calculation of these velocities is not sufficiently accurate. Borrowing from Weed, et al., a more accurate method was implemented which uses the residual expression to calculate the velocity ratio, V/U, under the assumption that the residual is zero at the surface points. The residual expression from FLO30 can be written in finite volume form as:

$$\mu_{\eta\zeta}\delta_\xi(\rho hU) + \mu_{\zeta\xi}\delta_\eta(\rho hV) + \mu_{\xi\eta}\delta_\zeta(\rho hW) + (\text{other terms}) = 0$$

The "other terms" in the above expression involve the grid point coupling and upwind dependence terms of the formulation and are assumed to be constants in the following development.

The desired velocities can also be written in this finite volume form as:

$$V = \rho hV = \mu_{\xi\eta\zeta}(\rho hV) \quad \text{and} \quad U = \rho hU = \mu_{\xi\eta\zeta}(\rho hU)$$

By simple manipulations, the normal velocity can be obtained from the residual expression as:

$$2\mu_{\xi\eta\zeta}(\rho hV) = 2\mu_{\zeta\xi}(\rho hV)_{\eta-1} - \mu_{\eta\zeta}\delta_\xi(\rho hU) - \mu_{\xi\eta}\delta_\zeta(\rho hW) - (\text{other terms}) \qquad (6)$$

where the subscript η-1 refers to the values at grid cell centers above the wing surface.

In order to use Eq. (6) to find the desired surface velocity ratio, it is necessary to know the U and W velocity components at the "ghost" cell centers below the wing surface. These values can be obtained in a manner consistent with FLO30 by specifying the "ghost" cell values to equal the values at corresponding points immediately above the wing surface. A comparison of the accuracy of both the finite difference approach and residual approach is shown in Figure 6. The calculated displacements are for a converged analysis solution for which the calculated slopes should of course be zero.

With the contravariant velocities known, an integration of Eq. (6) through the inverse design region from the leading edge to the trailing edge yields a set of surface displacements, $\delta(x)$, for the new wing surface relative to the previous one. These displacements are expressed as changes in the computational coordinate η, and are converted to surface displacements in the physical plane via the local grid transformation. The physical plane displacements are coincident with the

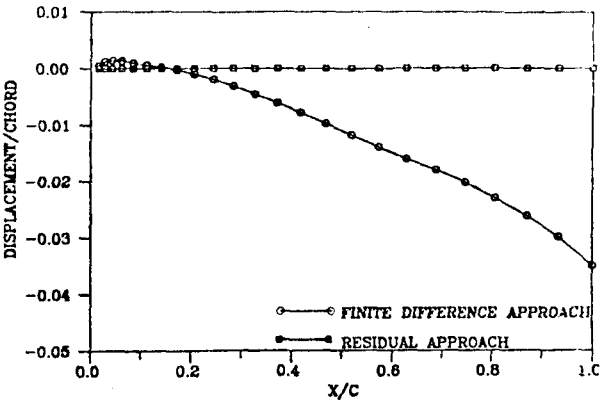

Figure 6. Comparison of Slope Calculation Methods

computational grid points in the inverse regions. To obtain the corresponding displacements at the original geometrical locations specified in the program input data, a linear interpolation of the above data is performed. Finding the displacements at the original geometry stations permits the calculation of the new wing airfoil sections at the same semispan locations.

Trailing Edge Closure

The procedures outlined above will compute a wing surface corresponding to a given, fixed, leading edge geometry and to a desired set of pressure distributions in the inverse regions. The above procedures do not, however, guarantee that this wing geometry will be practical. In particular, past experience[9] has shown that inverse surface calculations may yield airfoil sections which have either excessively blunt trailing edges or which, at least numerically, have the upper and lower surfaces crossed at the trailing edge ("fish tailed"). The former case is undesirable due to aerodynamic considerations, while the latter is physically impossible and may produce unpredictable problems in the grid generation or flow calculation portions of FLO30.

Since for any specified pressure distribution the corresponding wing surface will be controlled by the leading edge geometry, which serves as an initial spatial boundary condition for the inverse region, the problem of assuring trailing edge closure can be viewed as the proper selection of a leading edge shape. A procedure for systematically modifying the leading edge region in order to achieve some desired trailing edge thickness is called relofting. Such a relofting procedure has been incorporated into the present design process in order to both prevent the problems of trailing edge crossover and to allow the user the option of specifying a trailing edge thickness as an additional design variable. This design feature should be very useful in practical applications since it automates the iterative selection of a leading edge shape which would otherwise have to be performed by the user.

Two methods of relofting can presently be selected. The first method is a simple linear rotation scheme. This method can be visualized with the help of Figure 7. The dashed line indicates the original leading edge geometry and a hypothetical new surface shape which has been calculated for the inverse design regions. Without modification, this new surface has a trailing edge thickness of Δ. If a thickness of Δ_t were specified by the user, then the surface would have to be relofted or changed. In the present scheme, in order to obtain the

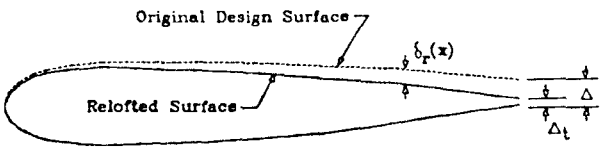

Figure 7. Relofting to Force Trailing Edge Closure

desired thickness, a displacement thickness, δ_r, is added to the current design surface. This thickness has a distribution from the leading to the trailing edge and is determined by the formula:

$$\delta_r(x) = (\Delta_t - \Delta)\ (x/c)$$

where c is the chord length of the local airfoil section. The total displacement for a surface update is then the sum of the two displacements, $\delta(x)$ and $\delta_r(x)$. When both the upper and lower surfaces are designed simultaneously, the displacement magnitudes determined by relofting are divided between the two surfaces so that half is added to the lower surface and half to the upper surface.

The second relofting method uses the same approach as the first for the aft inverse regions, but modifies the leading edge region by a proportional thining or thickening of the surface ordinates. This approach can be expressed by:

$$y^{n+1}(x) = y_j^{n+1}\ y^n(x) \ / \ y_j^n$$

where the j subscript refers to the ordinate at the direct-inverse junction determined from the linear relofting of the aft regions. Note that this method will produce leading edges in the same family of shapes and, for example, allow the design from a NACA 0012 airfoil to a NACA 0006 airfoil (see Test Case F).

RESULTS

A variety of different test cases were run as verification of the current design method. These cases involved both subcritical design and supercritical design over section geometries selected to test the versatility of the input and design control logic. In this section results from three of the more significant test cases will be presented. The results shown were obtained on a medium grid having 81 streamwise, 13 vertical, and 19 spanwise points with 11 spanwise stations and 53 points on the wing at each station; and in all cases the maximum change in the reduced potential was reduced at least three orders of magnitude. Thus, the results do not represent ultimate convergence but should be representative of "engineering accuracy".

The planform selected for the test cases was the Lockheed Wing A wing-body. The wing for this configuration has a quarter chord sweep of 25 deg., a linear twist distribution ranging from 2.28 deg. at the wing body junction to -2.04 deg. at the wing tip, an aspect ratio of eight, and a taper ratio of 0.4. The last two values are based upon the wing without fuselage. However, instead of the supercritical sections normally associated with Wing A, the initial airfoil sections at each span station were assumed to be composed of symmetric NACA four digit airfoil sections.

The target pressure distributions used in the design regions for the first two test cases were selected to yield airfoil shapes thicker in the aft portions of each section; and, at supercritical conditions, to yield on the upper surface weaker and more forward shock waves than those which would normally occur on a NACA 0012 section. On the lower surface, the target pressure distributions were selected to have either a favorable pressure gradient or fairly constant pressure plateau over much of the lower surface.

For the last test case, the pressure distribution was obtained from analysis solutions of an assumed wing geometry. The intent of this cases is to verify the relofting procedures and show the ability of the current method to make large surface changes in going from a thick wing to a thin wing (approximately 12 percent to 6 percent thick respectively).

All cases were for a freestream Mach number of 0.8 and an angle of attack of two degrees. In each case, the pressure distribution was specified in the design regions from the 15% local chord location to the trailing edge and used as the boundary condition in these inverse regions starting with the first iteration. Normally, three hundred SLOR iterations were executed prior to the first design surface update calculation; and subsequently, surface updates were computed every fifty cycles. Usually, the solution was considered converged and terminated after 550 total iterations for the first two cases and, due to the large amount of relofting required, after 950 iterations for the last case.

Test Case C

The inverse design regions for Case C, which was an attempt to design both upper and lower surfaces on two noncontiguous regions of the wing at supercritical conditions, are shown on Figure 8; and a comparison between the initial pressure distribution associated with NACA 0012 sections and the target pressures for two sections is portrayed on Figure 9. As can be seen, the target pressure distribution essentially eliminates at inboard stations the upper surface shock wave present on the original wing; and at outboard stations it weakens the shock and moves it forward. In addition, significant changes in the lower surface pressure gradients are evident. Also shown on Figure 9 are the pressures computed by the program at the end of the inverse design procedure (denoted as "design pressures"). These pressures are in excellent agreement with the target pressures, which indicates that the method is satisfying properly the desired inverse boundary conditions.

The corresponding designed airfoil sections for this case are shown on Figure 10. Even on the expanded scale, the agreement between the designed and target surfaces is excellent at all design stations. However, trailing edge closure was not enforced for this case; and there is at the boundary stations some departure between the designed surfaces and the target surfaces near the trailing edge. It is believed that this slight difference is a ramification of the change in spanwise slopes near the trailing edge between the direct and inverse regions.

In any event, the pressure distributions resulting from an analysis of the designed surfaces shown in Figure 10 are in excellent agreement with the target pressures, as can be seen on Figure 11. In addition, the section lift coefficients at the various design stations are in very good agreement with the target coefficients. Based upon these results it is believed that the present method can adequately design/modify nonadjacent regions of a wing in transonic flow.

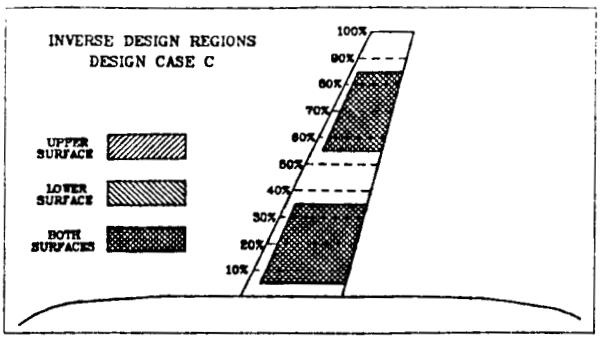

Figure 8. Design Case C

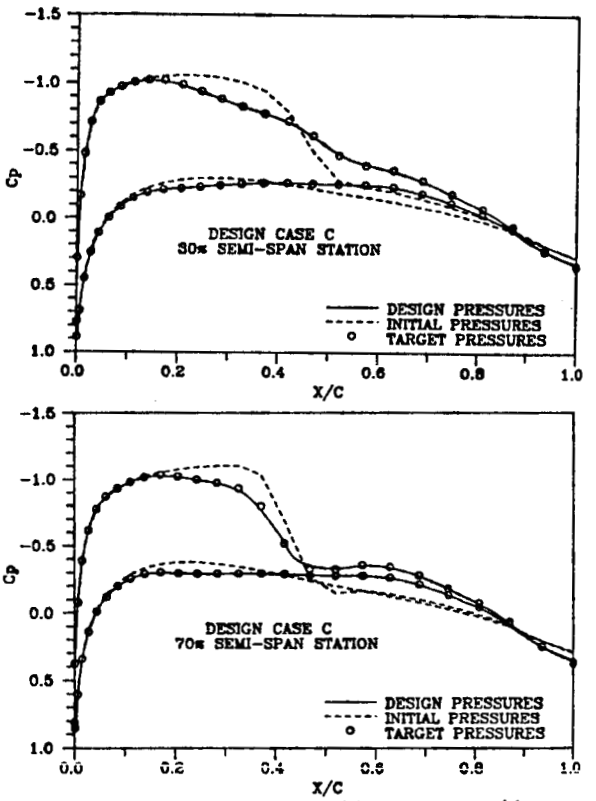

Figure 9. Comparison of Initial Pressures with Target Values (Case C)

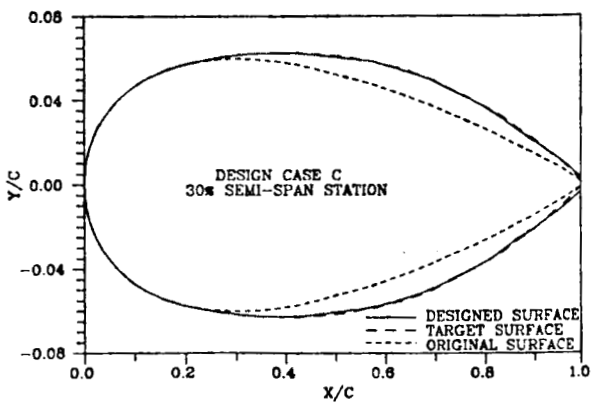

Figure 10. Comparison of Designed Sections with Original and Target Sections (Case C)

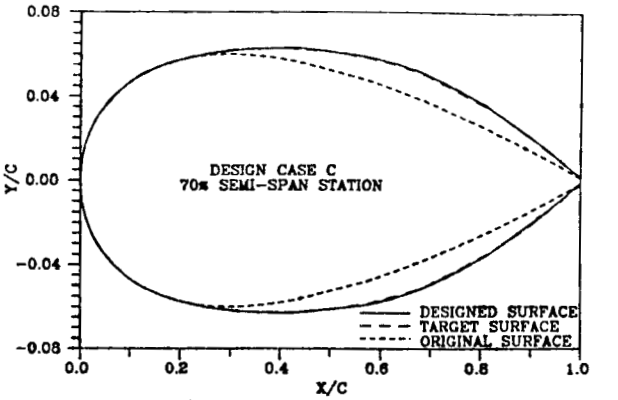

Figure 10. Continued

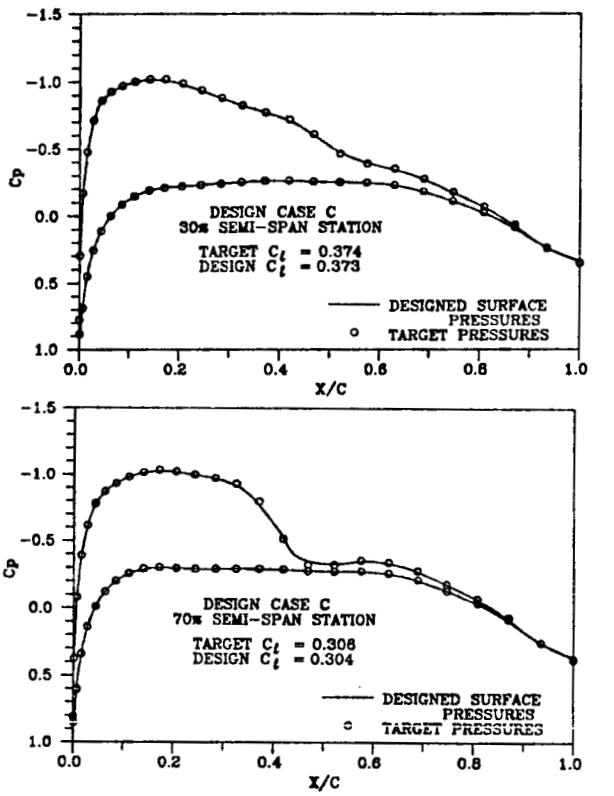

Figure 11. Comparison of Pressures from Analysis of Designed Wing Pressure Distributions (Case C)

Test Case E

For this test case, it was decided to design two non-adjacent upper surface regions simultaneously with a lower surface region which overlapped the upper zones. The location of these inverse design regions is shown on Figure 12. Likewise, Figure 13 compares the pressures associated with the initial wing sections shapes to the target pressures and to the pressures computed at the end of the design calculation for three design stations. It should be noted that this case is for supercritical condition and trailing edge closure is not enforced. As can be seen, at stations where only one surface is being designed (e.g. 50%, and 70%) the pressure distribution on the fixed surface also changes due to three dimensional effects from adjacent station which have been redesigned.

However, as depicted on Figure 14, only the design surfaces change form the original shape; and these surfaces are in reasonable agreement with the target profiles.

Finally, Figure 15 compares analysis results obtained for the designed wing with the target pressures. Even for this complicated case, the agreement between the two distributions and between the actual and target lift coefficients is excellent.

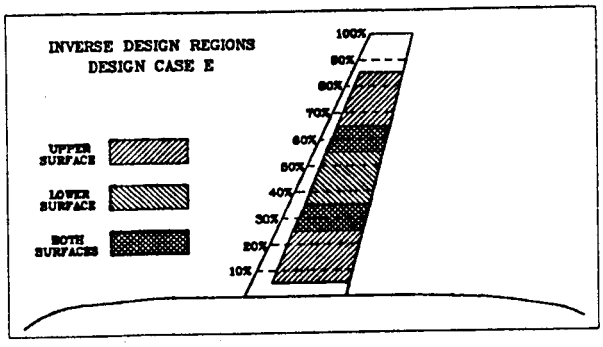

Figure 12. Design Case E

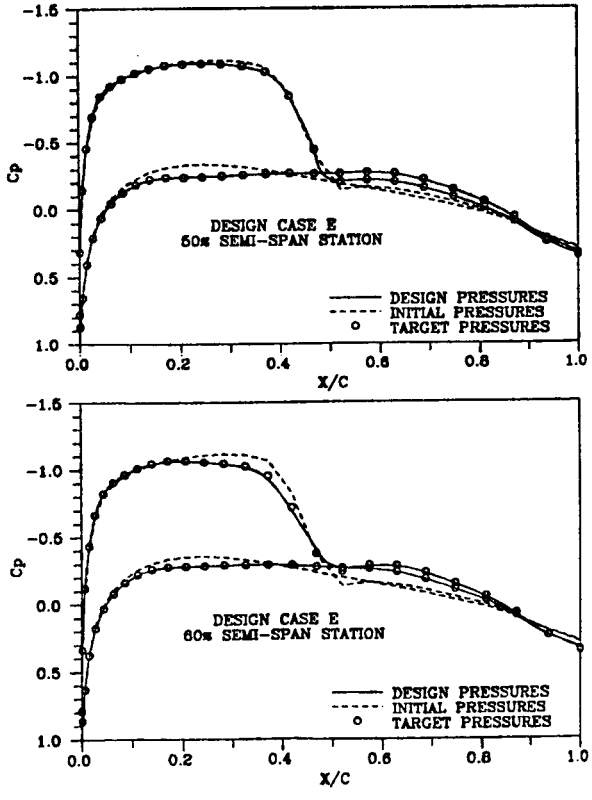

Figure 13. Comparison of Initial Pressures with Target Values (Case E)

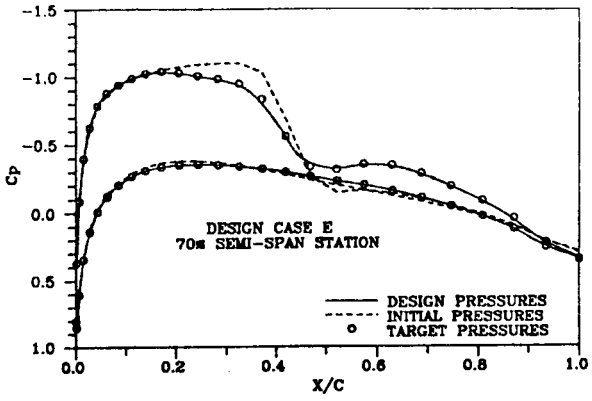

Figure 13. Continued

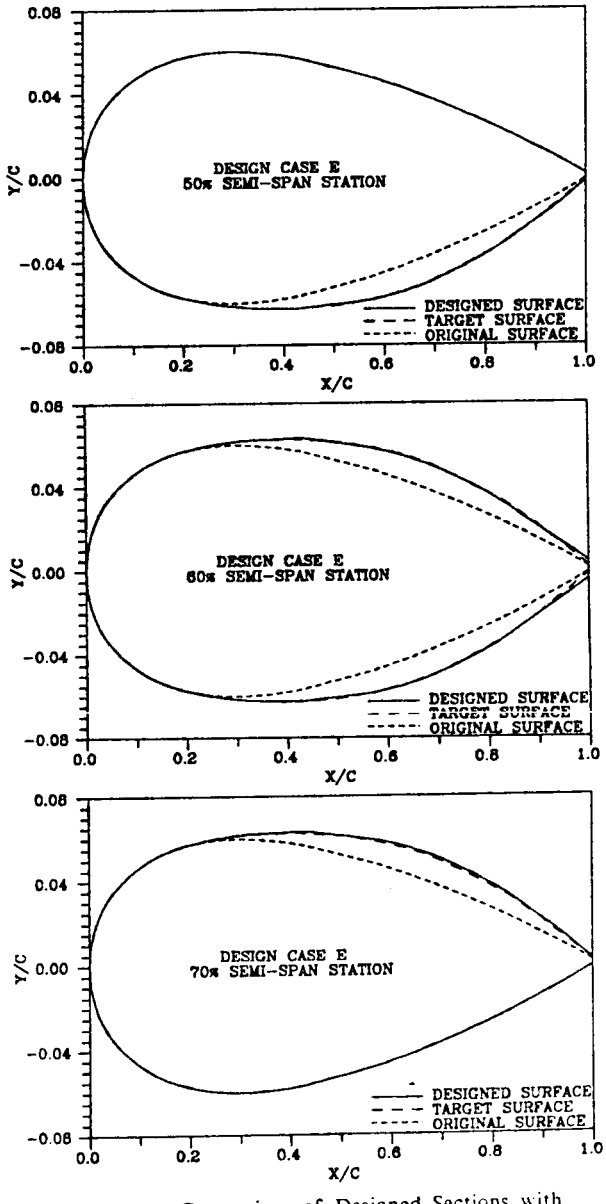

Figure 14. Comparison of Designed Sections with Original and Target Sections (Case E)

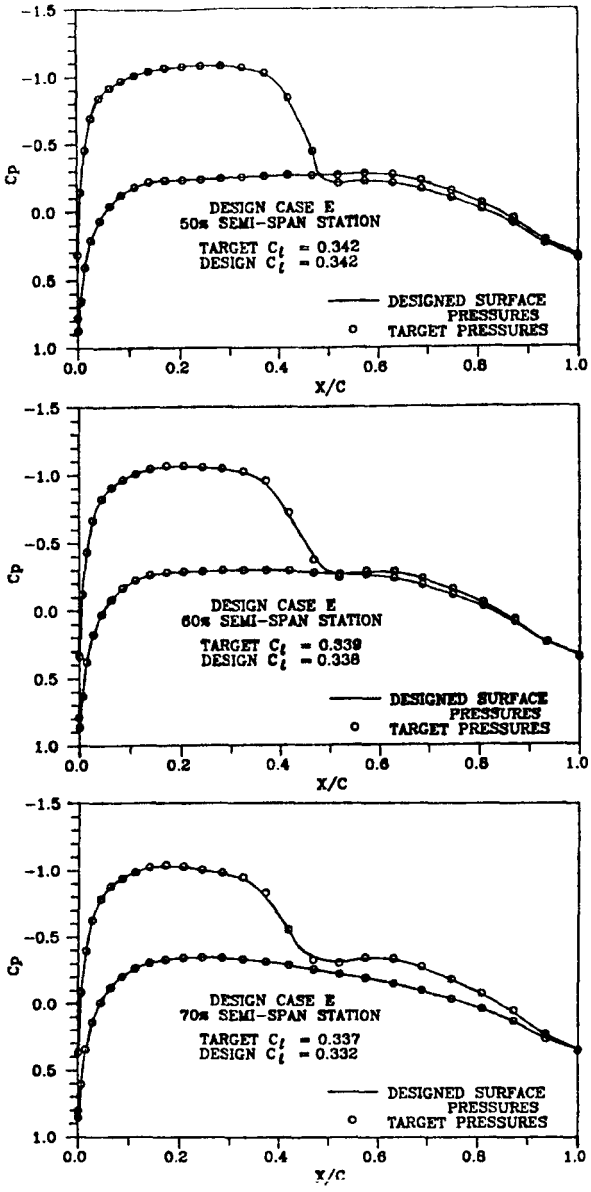

Figure 15. Comparison of Pressures from Analysis of Designed Wing Target Distributions (Case E)

TEST CASE F

The final test case was selected to demonstrate the ability of the design methodology to handle two difficult design tasks. The first task was to change a wing from super-critical to sub-critical. Due to the upstream dependance of the supersonic flow, this required making large changes in the leading edge region through the relofting procedures. The second task was to make large surface changes to the original airfoil without generating large surface distortions from the accumulation of geometry calculation errors. The design regions for this case are shown in Figure 16 where the wing thickness varied from 12% to 6% between the wing root and 80% span location and was constant going outward to the tip. The input design pressures were for a constant 6% thick wing.

The first attempts at this design used the linear leading edge relofting procedure and from a practical standpoint were unsuccessful. The final design surfaces were still supersonic in the leading edge regions while satisfying the subsonic aft surface conditions by producing strong shocks at the direct-inverse junction location. In addition, the surfaces themselves had sharp surface slope discontinuities at the same location.

When the thining approach was used to reloft the leading edge, much better solutions were obtained. Figures 17 through 19 show the changes in pressure distribution and surface shapes with a comparison of target to designed surface pressures for a few span sections as in the previous cases. As can be seen, excellent agreement between target and final pressures and surface were again attained for this extreme case. The only noticeable surface irregularities are a small wiggle at the direct-inverse junction which can also be seen as a small pressure jump in Figures 17 and 19.

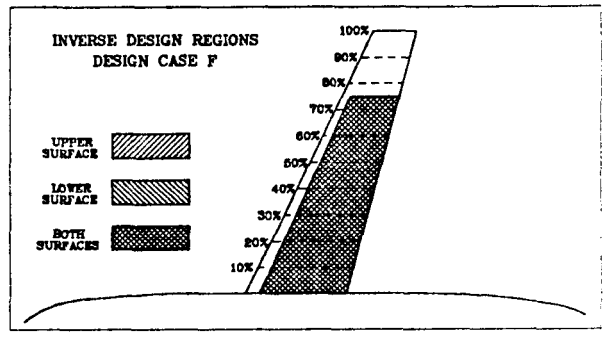

Figure 16. Design Case F

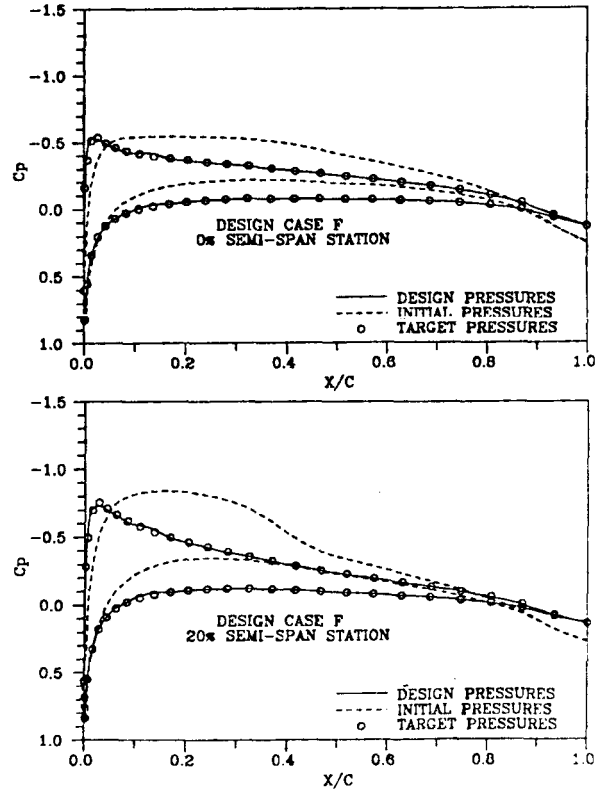

Figure 17. Comparison of Initial Pressures with Target Values (Case F)

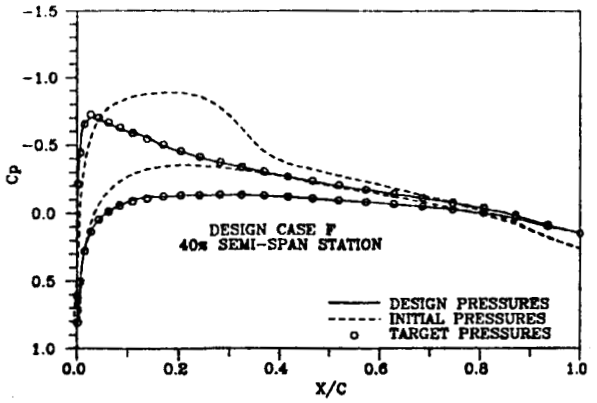

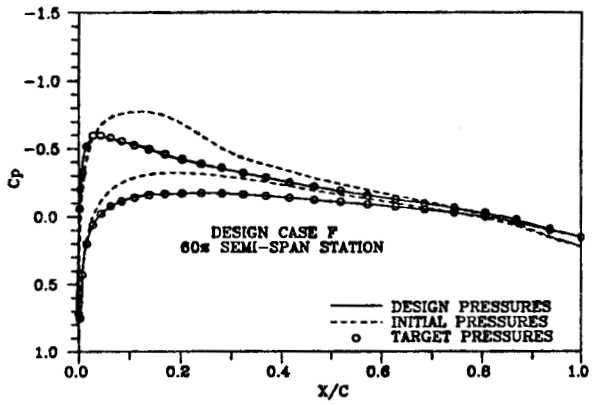

Figure 17. Continued

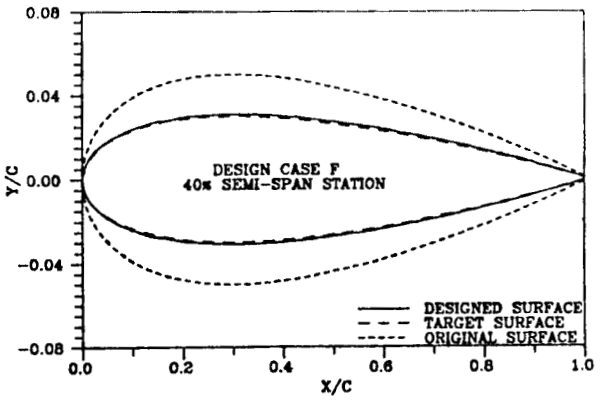

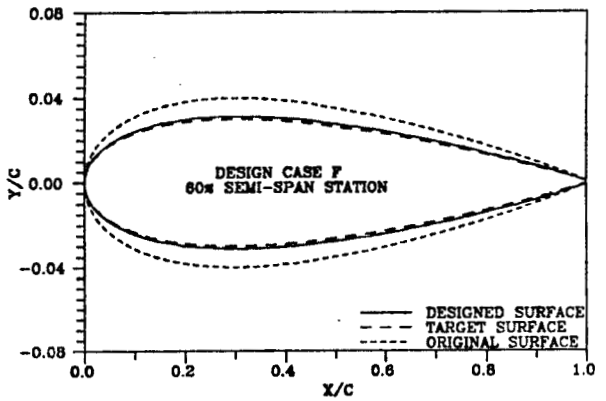

Figure 18. Continued

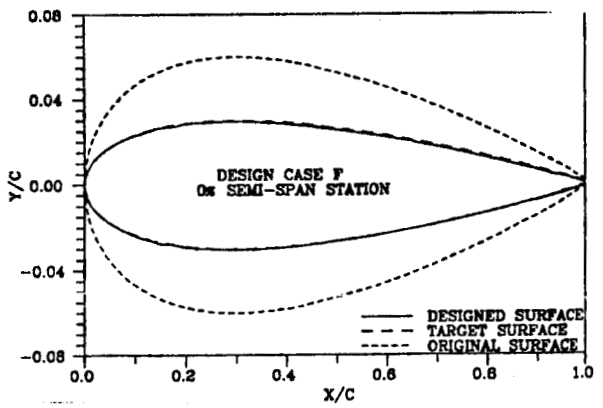

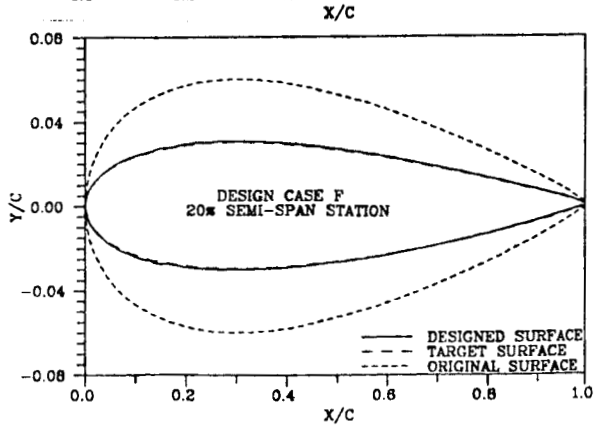

Figure 18. Comparison of Designed Sections with Original and Target Sections (Case F)

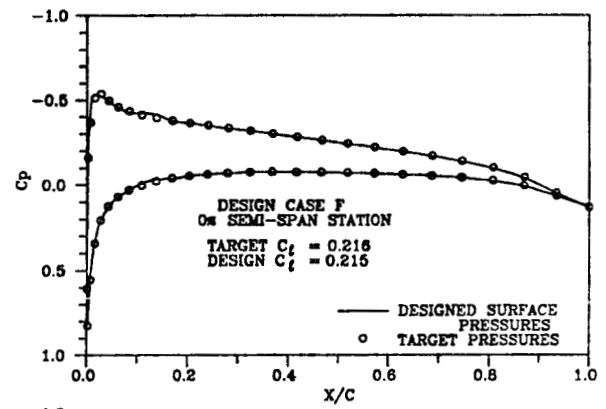

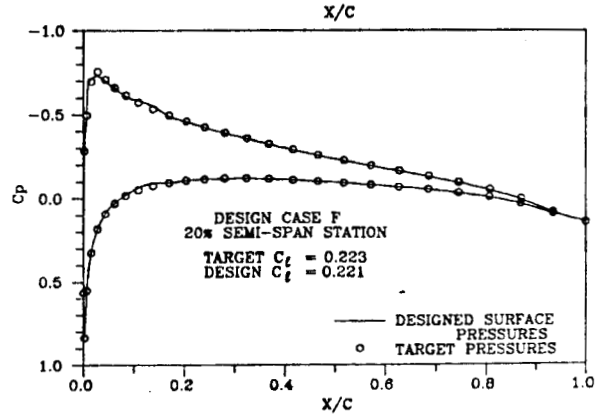

Figure 19. Comparison of Pressures from Analysis of Designed Wing Target Distributions (Case F)

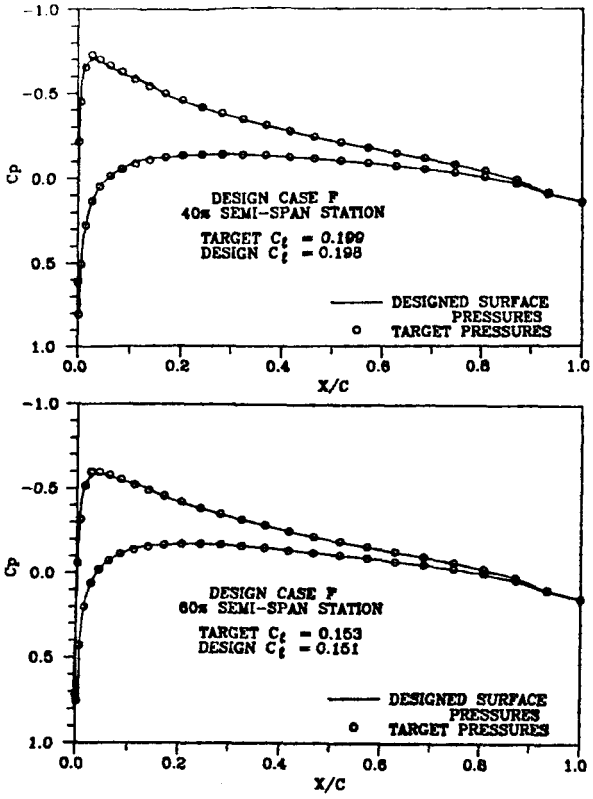

Figure 19. Continued

CONCLUSIONS AND SUGGESTIONS FOR FUTURE WORK

A direct-inverse wing design method has been successfully incorporated into the TAWFIVE transonic wing-body analysis computer code. The resultant code is capable of designing or modifying wings at both transonic and subsonic conditions and includes the effects of wing-body interactions. A series of test cases have been presented which demonstrate the accuracy and versatility of this inverse method.

Inclusion of viscous effects via the addition of the wing surface displacement thickness and wake thickness when performing wing design has been accomplished but not completely verified. Additional work will be required to run a sufficient sampling of test cases for evaluation of this design mode. The unique problems associated with viscous design and the effects of the various viscous correction models available in TAWFIVE would be the subject of a continuing research effort.

The development and evaluation of alternate methods of surface relofting are also topics for which continued research is suggested. The current method of relofting restricts the user to a family of leading edge geometries which can be constructed by the linear rotation of the initial shape. The option of using other relofting methods would extend the family of available shapes and add versatility to the design method.

ACKNOWLEDGMENTS

The work presented in this paper was primarily supported by the National Aeronautics and Space Administration under Grant NAG-1-619 with Richard L. Campbell of the Langley Research Center as technical monitor. The authors express their appreciation to Richard L. Campbell and Edgar Waggoner of NASA Langley for their assistance and helpful suggestions.

REFERENCES

1. Boppe, C. W., "Transonic Flow Field Analysis for Wing-Fuselage Configurations," NASA CR-3243, 1980.

2. Holst, Terry L. and Ballhaus, William F., "Fast, Conservative Schemes for the Full Potential Equation Applied to Transonic Flow," AIAA Journal, Vol. 17, No. 2, Febuary 1979.

3. Caughey, D. A. and Jameson, Anthony, "Progress in Finite-Volume Calculation for Wing-Fuselage Combinations," AIAA Paper 79-1513R, 1979.

4. Melson, N. D. and Streett, C. L., "TAWFIVE: A User's Guide," NASA TM84619, September 1983.

5. Cosentino, G. B. and Holst, T. L., "Numerical Optimization Design of Advanced Transonic Wing Configurations," AIAA Paper 85-0424, January 1985.

6. Davis, W., "TRO-2D: A Code for Rational Transonic Aero Optimization," AIAA Paper 85-0425, January 1985.

7. Bauer, F., Garabedian, P., and McFadden, G., "The NYU Inverse Swept Wing Code," NASA CR-3662, January 1983.

8. Tatsumi, S. and Takanashi, S., "Experimental Verification of Three-Dimensional Transonic Inverse Method," AIAA Paper 85-4077, October 1985.

9. Carlson, L. A., "Transonic Airfoil Design Using Cartesian Coordinates," NASA CR-2578, April 1976.

10. Carlson, L. A., "TRANDES: A Fortran Program for Transonic Airfoil Analysis or Design," NASA CR-2821, June 1977.

11. Anderson, W. K., and Carlson, L. A., "Inverse Transonic Wing Design on a Vector Processor," Texas A&M Research Foundation Report TAMRF-4535-8212, December 1982.

12. Weed, R. A., Anderson, W. K., and Carlson, L. A., "A Direct-Inverse Three-Dimensional Transonic Wing Design Method for Vector Computers," AIAA Paper 84-2156, August 1984.

13. Jameson, Anthony and Caughey, D. A., "A Finite Volume Method for Transonic Potential Flow Calculations," Proceedings of AIAA 3rd Computational Fluid Dynamics Conference, Albuquerque, N. M., June 1977, pp. 35-54.

14. Jameson, Anthony, "Iterative Solution of Transonic Flows over Airfoils and Wings, Including Flows at Mach 1," Comm. Pure Appl. Math., Vol. 27, 1974, pp. 283-309.

15. Jameson, Anthony, "Transonic Potential Flow Calculations Using Conservative Form," Proceedings of AIAA 2nd Computational Fluid Dynamics Conference, Hartfort, Conn., June 1975, pp.148-161.